THE OHIO STATE UNIVERSITY

SIMULATION OF AN ENHANCED TCAS II SYSTEM IN OPERATION

R.G. Rojas
P. Law
W.D. Burnside

The Ohio State University

ElectroScience Laboratory

Department of Electrical Engineering
Columbus, Ohio 43212

Semi-Annual Report 716199-9
Grant No. NSG 1498
October 1987

National Aeronautics and Space Administration
Langley Research Center
Hampton, Virginia 23665

NOTICES

When Government drawings, specifications, or other data are used for any purpose other than in connection with a definitely related Government procurement operation, the United States Government thereby incurs no responsibility nor any obligation whatsoever, and the fact that the Government may have formulated, furnished, or in any way supplied the said drawings, specifications, or other data, is not to be regarded by implication or otherwise as in any manner licensing the holder or any other person or corporation, or conveying any rights or permission to manufacture, use, or sell any patented invention that may in any way be related thereto.

50272-101

REPORT DOCUMENTATION PAGE	1. REPORT NO.	2.	3. Recipient's Accession No.

4. Title and Subtitle SIMULATION OF AN ENHANCED TCAS II SYSTEM IN OPERATION	5. Report Date October 1987 6.
7. Author(s) R.G. Rojas, P. Law, W.D. Burnside	8. Performing Organization Rept. No. 716199-9
9. Performing Organization Name and Address The Ohio State University ElectroScience Laboratory 1320 Kinnear Road Columbus, Ohio 43212	10. Project/Task/Work Unit No. 11. Contract(C) or Grant(G) No. (C) (G) NSG 1498
12. Sponsoring Organization Name and Address National Aeronautics and Space Administration Langley Research Center Hampton, Virginia 23665	13. Type of Report & Period Covered Semi-Annual 14.

15. Supplementary Notes

16. Abstract (Limit: 200 words)

This study describes the computer simulation of a Boeing 737 aircraft equipped with an enhanced Traffic and Collision Avoidance System (TCAS II). In particular, an algorithm is developed which permits the computer simulation of the tracking of a target airplane by a Boeing 737 which has a TCAS II array mounted on top of its fuselage.

This algorithm has four main components; namely, the target path, the noise source, the alpha-beta filter and the threat detecting algorithm. The implementation of each of these four components is described in this report. Furthermore, the areas where the present algorithm needs to be improved are also mentioned.

17. Document Analysis a. Descriptors

b. Identifiers/Open-Ended Terms

c. COSATI Field/Group

18. Availability Statement	19. Security Class (This Report) Unclassified	21. No. of Pages 80
	20. Security Class (This Page) Unclassified	22. Price

(See ANSI-Z39.18) See Instructions on Reverse OPTIONAL FORM 272 (4-77)
(Formerly NTIS-35)
Department of Commerce

TABLE OF CONTENTS

LIST OF TABLES

LIST OF FIGURES

I. INTRODUCTION

This report describes the computer simulation of an Enhanced TCAS II antenna tracking a single target when it is mounted on top of the fuselage of a Boeing 737 aircraft. The performance of a TCAS II system can be negatively affected by many different aspects, such as interference, hardware-related errors, thermal noise, stability of the inertial navigation system, the distortion of antenna patterns by own aircraft, etc. This report primarily investigates the structural scattering effects of a Boeing 737 on a TCAS II antenna in terms of angular and miss distance errors. Angular and miss distance errors are of primary concern here because angular errors, after filtering, directly affect the accuracy of miss distance detection. Furthermore, the greater the uncertainty of miss distance detection, the greater are the threshold levels required to detect any threat of collision, which in turn can lead to more false alarms.

The OSU aircraft code [1] is used to generate two sets of monopulse characteristic curves. The first set is generated with the TCAS II array mounted on the fuselage of a Boeing 737 with no wings and tail attached, and it will be referred to as the **lookup table**. The second set is generated by adding two wings and a vertical stabilizer to the above simulated model. This way, a more realistic model is used for the aircraft. The data obtained from the second set is entered to the lookup table to obtain the detected bearing angles of the target with respect to the protected aircraft. Furthermore, the error budget estimated by Sinsky and Tier in Reference [2] is also used to simulate noise. With this simulated noise and the two sets of monopulse

characteristic curves, a more accurate model of the TCAS II system can be constructed. Thus, all the sources of error are divided into two groups; namely, structural scattering and a noise generator which combines all the sources of error besides structural scattering. It is noted that the simulation can be displayed in color with the Graphical Kernal System (GKS). The color display shows real and detected target locations on the Tektronix 4129 terminal which are updated every second. The real and detected time to the closest point of approach (time to CPA), the horizontal miss distance, the speed and the relative height of the target are also displayed on the graphics terminal. The equations used to calculate the miss distance, time to CPA and the speed of the target are given in Section II. A more detailed discussion of these equations can be found in [2-5].

II. SIMULATION

Our simulation involves the tracking of a single target approaching the protected aircraft. The path of the target is arbitrary and it can be changed when the program is being run. The simulation of a TCAS II array mounted on a Boeing 737 has been reported in [6-8] and it will not be discussed here. This report deals with the simulation of a target path, noise, the alpha beta filter and the threat detecting algorithm. These four components are the most important in our computer model. It is noted that each one can affect the performances of the TCAS II system, and thus, it is necessary to carefully study them.

The alpha beta filter minimizes the effect of noise, and it also gives an estimate of the target's present position, the predicted

position and its velocity. Moreover, the threat detecting algorithm depends on the output of this filter. Thus, the number of false alarms does not only depend on how severe the noise is, but also on how well the filter smooths the noise.

The Enhanced TCAS II system has two arrays: one mounted on the top of the fuselage and the other on the bottom of the fuselage. The top mounted antenna is supposed to search for targets located above the aircraft while the bottom one searches targets below the aircraft. Without loss of generality, only the **top mounted antenna** is simulated in this report. The same procedure as described here can be followed to simulate the bottom mounted antenna. However, since the computer model of the aircraft depends on the antenna location, the computer model of the aircraft for the bottom mounted antenna will be different from the one used for the top mounted antenna.

Two sets of monopulse curves are used to study the scattering effects of the wings and the vertical stabilizer. Each set consists of 8 monopulse curves covering the azimuth plane at a fixed elevation angle. Since there are 8 beam positions, each monopulse curve is responsible for an azimuth sector of 45 0°. Monopulse characteristic curves [4,6] are calculated at 15 elevation angles covering angles of 0, 1, 2, 3, 4, 5, 6, 7, 8, 9, 10, 15, 20, 25 and 30 degrees. If the target elevation is between two of the above angles, its azimuth angle is determined by averaging the two azimuth angles corresponding to these two elevation angles. Furthermore, if the target elevation is above 30°, the monopulse curve corresponding to 30° is used. As an example, Figure 1 shows a pair of monopulse curves. If the monopulse receiver

reads a value of 4 dB, corresponding to a target bearing of 1° off boresight, the lookup monopulse curve indicates that the detected target bearing is about 7° off boresight. Thus, the error due to the structural scattering of the protected aircraft is about 6° for this particular case.

A. Simulation of a Target Path

Although only the last 40 seconds of the target's flight path are shown on the Tektronix 4129 terminal, our computer model tracks a target for 60 seconds before the CPA. In our simulation, there is no restriction of the distance of the target from the protected aircraft. As mentioned before, the display routine is written in GKS language where the real and detected target locations are updated every second. Furthermore, the threshold boundaries are also shown on the screen. An example of this display can be seen in the next section, i.e., in Figures 27, 35, 53 and 55. Appendix 1 defines each symbol and the color-code used in these figures.

The coordinate system used in this routine is fixed with the protected aircraft. Thus, all the input data is understood to be referred to this coordinate system. The inputs to the program are the height, the speed and the starting position of the target. In addition to these data, the parameters of an arbitrarily oriented straight line (target's path) are also needed. Note that a curved path can also be read in from a data file. Likewise, noise can be simulated by the program or it can be read in from outside. The target's path, speed and height can be changed during the last 40 seconds of the simulated

flight. The program then calculates the target's bearing, bearing rate, miss distance and time to CPA; however, the last three parameters are not accurate for a curved path since they are calculated assuming a straight path. When the path is straight, the exact and calculated parameters are compared to obtain errors incurred in calculating these parameters. If the target poses a threat, the program gives a warning, and a subsequent escape path can be executed. The target poses a threat when the calculated miss distance is within the threshold curves.

B. Noise Simulation

In order to have a more realistic model of the TCAS II system, noise is also included in our computer model. Sinsky and Tier [2] found that there are four main sources of error in the TCAS II system; namely, hardware-related errors, structural scattering, thermal noise and errors introduced by the inertial navigation system. A summary of these sources of error is depicted in Figure 2. It is also shown in [2] that the standard deviation of the bearing error σ_B falls between 1.4° and 2.8°, depending on the transponder reply signal-to-noise ratio S/N. Table 1 gives values relating S/N to transponder power and target range. It turns out that

$$S/N = 10^{(S/N)_o/10 - 2\log_{10}(R/R_o)} \qquad (1)$$

Table 1

Signal to Noise Ratio for Two Power Levels
of the Target's Transponder Transmitted Power
(Obtained from Ref. [2])

Transponder Power	Signal-to-Noise Ratio $(S/N)_o$	Distance R_o
18.5 dBω	17.9 dB	20 NM_i
27 dBω	26.4 dB	20 NM_i

where $(S/N)_o$ and R_o are defined in Table 1. It is noted that $(S/N)_o$ in Equation (1) is given in dBs and the target range R in nautical miles.

All the errors mentioned above can be combined to obtain the following expression [2]

$$\sigma_B = \left(1.13^2 \left(0.97^2 + \frac{(0.35 \times 64)^2}{S/N} + 0.71^2\right) + 0.14^2\right)^{1/2} \qquad (2)$$

In Equation (2), 0.71° is the contribution from the structural scattering. This value was calculated in [2] assuming that targets are uniformly distributed in angle 360° around the protected aircraft. In our simulation, the error introduced by structural scattering is determined by the two sets of monopulse curves defined in the introduction. Thus, structural scattering introduces deterministic and not statistical errors. Therefore, the noise that is simulated in our program is assumed to be Gaussian noise with zero mean and with a standard deviation given by

$$\sigma_B = \left(1.13^2 \left(0.97^2 + \frac{(0.35 \times 64)^2}{S/N}\right) + 0.14^2\right)^{\frac{1}{2}} . \qquad (3)$$

Equations (2) and (3) are plotted in Figure 3 to show the effects of the estimated scattering error as the target range changes. It can be seen that in general the structural scattering contributes to the errors in detecting the target bearing; however, when the target range increases, the scattering effects becomes less significant as the noise will dominate the overall angle detection accuracy.

C. Simulation of the Alpha Beta Filter

According to Sinsky [5], the function of an alpha beta filter is to accept samples of the target position and to filter this data so that the resulting output samples are the smoothed estimates of the present position, the predicted position and the velocity of the target. These filter characteristics have been optimized in the TCAS II system so that the uncorrelated errors are minimized, while the filter can still be fast enough to detect changes in the target path. The optimized alpha beta filter parameters represent a compromise between noise reduction on one hand and target tracking on the other. The parameters used for the filter are α=0.25 and β=0.066. The alpha beta filter implemented here can be defined by the following difference equations [5]

$$\bar{X}_k = X_{pk} + \alpha(X_k - X_{pk}) \qquad (4)$$

$$\bar{\dot{X}}_k = \bar{\dot{X}}_{k-1} + \frac{\beta}{T}(X_k - X_{pk}) \qquad (5)$$

$$X_{p(k+1)} = \bar{X}_k + T\,\bar{\dot{X}}_k \tag{6}$$

where

T = sampling time interval which is 1 second in this case

X_k = k^{th} measurement of X

$\bar{X}_k$ = smoothed estimate of X at the k^{th} time index

$\bar{\dot{X}}_k$ = smoothed estimate of $\dot{X}$ at the k^{th} time index

X_{pk} = predicted value of X at the k^{th} time index.

Note that $\dot{X}$ is the derivative of X with respect to time. The filter output determines the bearing rate $\dot{B}_k$, which is given by the following equation [2]

$$\dot{B}_k = \frac{\left(\bar{X}_k \bar{\dot{Y}}_k - \bar{Y}_k \bar{\dot{X}}_k\right)}{\left(\bar{X}_k^2 + \bar{Y}_k^2\right)} \tag{7}$$

The bearing rate can be translated directly into horizontal miss distance estimation, denoted by M_k in this report, which is given by [3]

$$M_k = \left[\frac{\left(\bar{X}_k^2 + \bar{Y}_k^2\right)}{\sqrt{\bar{\dot{X}}_k^2 + \bar{\dot{Y}}_k^2}}\right] \dot{B}_k \tag{8}$$

It can be shown that for collision courses or near collision courses, the time to CPA, τ_k, can be approximately expressed as [2]

$$\tau_k = \frac{\sqrt{\bar{X}_k^2 + \bar{Y}_k^2}}{\sqrt{\dot{\bar{X}}_k^2 + \dot{\bar{Y}}_k^2}} \quad . \tag{9}$$

Combining Equations (8) and (9), the miss distance estimation for a collision or a near collision course can be rewritten as [3]

$$M_k = \sqrt{\bar{X}_k^2 + \bar{Y}_k^2}\ \dot{B}_k \tau_k = \sqrt{\dot{\bar{X}}_k^2 + \dot{\bar{Y}}_k^2}\ \tau_k \dot{B}_k \quad . \tag{10}$$

The miss distance error δM_k can then be approximated by estimating the bearing rate error. It follows from Equation (10) that

$$\delta M_k \simeq \sqrt{\bar{X}_k^2 + \bar{Y}_k^2}\ \tau_k\ \delta\dot{B}_k = \sqrt{\dot{\bar{X}}_k^2 + \dot{\bar{Y}}_k^2}\ \tau_k^2\ \delta\dot{B}_k \quad . \tag{11}$$

The above equation holds only when reasonable estimates on $\sqrt{\bar{X}_k^2 + \bar{Y}_k^2}$ and $\sqrt{\dot{\bar{X}}_k^2 + \dot{\bar{Y}}_k^2}$ are available. Since miss distance error is closely related to the bearing rate error, it is important to study the sources of bearing rate error. For completeness, a summary of the sources of bearing rate error are given in Figure 4. All the details about Figure 4 can be found in [2].

D. Simulation of the Threat Detecting Algorithm

The most important result in Section C is Equation (11). This equation indicates that the error in estimating horizontal miss distance is directly proportional to the error in estimating the bearing rate, provided the estimates of τ_k and $\sqrt{\bar{\dot{X}}_k^2 + \bar{\dot{Y}}_k^2}$ are reasonable. Furthermore, according to Sinsky and Tier [2], if the target's horizontal miss distance is at least three times the one-sigma uncertainty in miss distance, then collision avoidance is virtually assured. Thus, the effectiveness of the threshold depends on how accurate the estimate of the bearing rate is. The variance of the bearing rate error is computed in [2] and only the final expression is given here, namely:

$$\sigma_{\dot{B}} = \left\{\left\{0.01\left[0.36^2 + \frac{(0.35 \times 64)^2}{S/N}\right] + (0.71 \times 0.081)^2\right\}1.13^2 + 0.000138^2(0.35^2 + 0.35^2 + 1.)\right\}^{1/2} \qquad (12)$$

where S/N was defined in (1). It follows from (11) that the variance of the horizontal miss distance (σ_m) can be written the following way:

$$\sigma_m \tilde{\sim} \sqrt{\bar{\dot{X}} + \bar{\dot{Y}}}\ \tau^2\ \sigma_{\dot{B}} \qquad (13)$$

In our model, the threshold for horizontal miss distance is set at three times the variance of the miss distance estimation error given in Equation (13), plus a safety margin of 1000 ft. When the detected miss

distance is less than the threshold level, there is a potential for collision. The program then checks the relative height of the target. If its relative height is less than 300 ft., a warning is issued and a subsequent escape curve can be taken. In this report, one of three escape curves obtained from Reference [9] can be chosen, namely the 10 second rollover to 30° path, the 6 second rollover to 45° path and the 6 second rollover to 30° path. When the plane follows one of these escape curves shown in Figure 5 at 275 knots, it will accelerate laterally to avoid a collision. Note that when an aircraft takes on any curved path, it will roll due to the centrifugal force acting on it. Thus, the rolling of an aircraft will change the relative target position with respect to the turning aircraft. In our present computer model, this rolling effect has not yet been included; however, this will be our next step in this research effort.

When the detected miss distance lies within the threshold boundaries, an alarm is given. If the aircraft then follows an escape curve, the detected miss distance can be brought out of the threshold region which will then set off the alarm. Examples on this will be shown in the next section. For further application, this program can be used to test various threshold equations in order to reduce the number of false alarms and yet not increase the risk of collision.

III. RESULTS OF SIMULATION

The objective of this section is to investigate how the structural scattering and noise affects the ability of the TCAS II system to accurately estimate the target bearing and the miss distance at CPA when

a TCAS II equipped Boeing 737 is approached by an intruder. In this report, the intruder takes on two simulated flight paths, i.e., Path One and Path Two, as shown in Figure 6. The coordinate system used here is defined in Figure 7. The intruder's location can be represented in the spherical coordinates (r,θ,ϕ) with respect to the Boeing 737. When their separation r is small enough so that the magnitude of the noise is small, the scattering errors depend on the intruder's azimuth and the angles θ and ϕ. That is, the errors are mainly due to the structural scattering. On the other hand, if r is larger, the errors due to noise become dominant. The next section examines the bearing and elevation angle errors caused by the scattered field as a function of azimuth and elevation angles. It is important to emphasize that in Section A errors due to noise are not taken into account.

A. Bearing and Elevation Angle Errors due to Structural Scattering

Before the bearing error curves are shown, it is important to define the convention used to measure this error. Figure 8 depicts the convention used in this report. Furthermore, the top-mounted TCAS II antenna is located on the centerline of the fuselage of a Boeing 737, about 35 ft. from the nose. Figures 9 through 15 show the bearing errors when a target's azimuth angle changes. Note that each figure corresponds to a different elevation angle. As an analogy to a real situation, the target can be seen as circling around the Boeing 737 at a constant radius and elevation angle. Each figure also consists of two graphs with the top graph designated as Figure (a) and the bottom graph as Figure (b). The top graphs in Figures 9 through 15 are the bearing

error curves obtained by using 64 beam positions of the top mounted antenna. The bottom graphs are obtained by using 8 beam positions of the top mounted array. In other words, each beam position in the top graph covers an azimuth sector of 5.625 degrees while that in the bottom graph covers a sector of 45°. It can be seen from Figures 9 through 15 that the bearing errors are generally reduced by using 64 beam positions. Moreover, Figures 9 through 15 show that the bearing errors are more severe when the beams are pointed in the vicinity of the tail of the aircraft. Furthermore, as pointed out in [6], when the elevation angle is between 0° and 22°, the direct field radiated by the array will be blocked by the vertical stabilizer which results in more severe bearing errors as shown by Figures 9 and 10. Figures 13 through 15 show the bearing errors when the target is below the protected aircraft. It can be seen that the bearing errors increased as the elevation angle decreases. As an example, for the case with 64 beams, the standard deviation of the bearing error curve changed from 0.637° at 30° elevation to 11.4° at -30° elevation. This means that if only the top mounted antenna is used, the rolling of an aircraft will affect the detection of a target significantly. These seven figures also illustrate that the bearing errors are anti-symmetric about the azimuth angle of 180° when the TCAS II antenna is mounted on the centerline of the fuselage and the bearing error is measured as depicted in Figure 8.

Figures 16 through 20 show the bearing errors as the target's elevation angle changes. Each figures corresponds to a different azimuth angle. It can be seen that when the azimuth angle of a target is less than 35°, i.e., around the nose section, the bearing error is

smooth and relatively small. However, when the target is behind the aircraft and it shadowed by the tail, the bearing error is rough and more severe. Of particular interest is Figure 17, where the azimuth angle is 32.24°, because it can serve as a bearing error lookup table for flight Path One. Since this path represents a target coming in at a constant azimuth angle of 32.24°, Figure 17 can be used to find the scattering error as the target approaches on Path One.

B. Simulation of TCAS II Antenna Tracking a Target

Figures 21 through 49 show our simulation results on flight Paths One and Two. These results can be divided into four sets of figures such that the first set is from Figures 21 through 27; the second set is from 28 through 35; the third and fourth sets are Figures 36 through 42 and 43 through 49, respectively. The first set of figures depicts simulation results on flight Path One when only scattering effects are included. The second set of figures includes random noise which is not taken into account in the first set. The third and fourth sets of figures are simulation results on flight Path Two. They are obtained based on the same logic as the first two sets of figures.

The effect of structural scattering on the system performance, such as miss distance detection, can be examined by separating scattering errors from the overall system errors. Furthermore, since noise is generated at random with a standard deviation given by Equation (3), all the simulation results will change depending on the noise added. For comparison purposes, one particular noise curve, shown in Figure 28, is chosen for Paths One and Two. In addition to Figure 28, four other

noise curves and their corresponding miss distance curves are shown from Figures 55 through 62. The following sections will study and interpret each set of figures.

1. Scattering Effects on Path One

One reason for choosing Path One is because this path was used by Bendix to conduct a series of flight tests. Some of the measurements are available in References [4,9] for comparison. Another reason is that if the target approaches at a constant azimuth angle, the scattering effects are due to a change of the target's elevation which can be examined in detail.

Figures 21 through 27 show simulation results on this path which include the real and detected target bearing, bearing rates, bearing errors, bearing rate errors, miss distance and miss distance errors. Figure 27 shows the color display of the Tektronix terminal. The miss distance error in this case is less than 20 meters and the standard deviation of the bearing error curve is 0.291° (see Figure 23). The bearing rate is singular at the origin (see Equation (7)) which can be seen in Figure 24 where the bearing rate error curve is shown. As stated before, this path shows the scattering effects due to the target's change of elevation angles for a fixed azimuth angle. These scattering effects are small (for elevation angles between 0° and 30°) when compared to those due to a change of azimuth angles as will be shown later on Path Two.

2. Noise and Scattering Effects on Path One

Simulated noise, as shown in Figure 28, is added to the previous case. This noise is generated by a Gaussian noise routine where $(S/N)_o$=26.4 dB and R_o=20 NM_i, corresponding to a transponder power of 27 dBω (see Table 1), was used in Equation (3) to calculate σ_B. The results of this simulation are shown in Figures 29 through 35. When compared to the last case, the miss distance error and the bearing error curves are affected the most after the noise was added. The threshold curves do not change since they are determined by Equation (13) (see Section IIC) and are independent of the noise added. The miss distance errors attain a maximum of 1250 meters; a 63-fold increase when compared to the preceding case. The standard deviation of the bearing error curve also increases from 0.291° to 1.71°. The errors due to the scattered fields are almost negligible after noise is added. The corresponding color graphic display is shown in Figure 35.

3. Scattering Effects on Path Two

Path Two is chosen for a target approaching the Boeing 737 from behind. The scattering errors on this path are worse than those on Path One due to the strong shadowing by the vertical stabilizer. Moreover, the target continuously changes its azimuth and elevation angles as it approaches the Boeing 737. The scattering effects examined in this case are mainly due to a target's change of its azimuth angles. For comparison purposes, the relative target speed and height are the same as those in the previous two cases. Figures 36 through 42 show the results on this path. The bearing error curve in Figure 38 is cyclic in

nature with a standard deviation of 0.524°. The miss distance error curve shown in Figure 41 also fluctuates as a function of the time to CPA. This error curve takes the shape of a damped harmonic with a maximum magnitude of 750 meters. Figure 42 depicts the graphic display of this path. All along, the TCAS II system predicts that the target is not on a collision course since the detected miss distance curve is not bounded by the threshold curves.

4. Noise and Scattering Effects on Path Two

The same simulated noise as depicted in Figure 28 is added to Path Two. Figures 43 through 49 show the results of this simulation. Comparing Figures 41 and 48, it can be seen that the addition of noise greatly affects the miss distance curve. A false alarm could have resulted if a decision would have been made between -40 and -39 seconds as shown in Figure 47. The color graphic display for this path is shown in Figure 49. Figures 50 and 51 depict the miss distance and its error curves caused by the added noise alone. Comparing Figures 41, 48 and 51, it can be seen that the shape of the miss distance curve is generally determined by the noise added, provided that the standard deviation of the added noise is greater than that of the scattering errors. The standard deviation of the bearing error curve increases from 0.524° to 1.85° after noise is added.

C. Escape Curves

Each of the four color graphic displays depicted in Figures 27, 35, 42 and 49 shows a set of escape curves. These escape curves are some of

the possible paths that a TCAS II equipped aircraft can take to avoid a collision. However, as to which escape curve is followed by the protected aircraft will depend on the protected aircraft's ability to maneuver. This section examines the tracking of a target when it follows an escape curve. As mentioned earlier, the rolling of an aircraft when it changes bearing is not yet included in our present model. The error will increase when this rolling is taken into account, especially when only a top mounted antenna is used. Note that since the coordinate system used here is fixed with the protected aircraft, the escape curves shown in Figures 27, 35, 42 and 49 indicate the possible escape curves followed by the target instead of the TCAS II aircraft.

The solid light blue line in Figure 35 represents an escape curve of "6 seconds rollover to 45°". It can be seen from this figure that if the target takes this path, the alarm will be turned off 24 seconds before the predicted collision. Figure 52 shows the tracking of a target when it actually takes this escape curve. The difference between Figures 35 and 52 is that in Figure 35, the target does not change its straight path although an escape curve predicts a safe path is possible. On the other hand, Figure 52 shows the tracking of a target after it has taken the escape path. Figures 52 and 53 show that the detected miss distance is increased by the target's horizontal maneuver. Because of this increase, the magnitude of the detected miss distance is larger than the magnitude of the threshold at some point before CPA which means that the alarm is then turned off. Figure 54 shows the tracking of a target, which originally started on Path Two, as it follows the escape curve "6 seconds rollover to 45°". It can be seen from Figures 52 and

54 that the detected target location-curve follows quite well the real target location-curve.

D. Some Other Simulation Results on Path One

Figure 55 through 62 show simulation results on Path One when four other noise curves are added. It can be seen that the threshold curves shown in Figures 58 and 60 are not large enough to ensure one hundred percent threat detection for the two particular noise curves added. Figure 61 shows a noise curve with a standard deviation of 0.6°. The corresponding miss distance error curve, depicted in Figure 62, agrees very well with the measured data shown in Figure 63. It is noted that in all the noise curves shown in Figure 55, 57, 59 and 61, $(S/N)_o$= 26.4 dBw and R_o=20 NM_i.

E. The Effect of a Constant Angle Error

A constant angle of 2° is added to the noise curve shown in Figure 28 and the resulting noise curve is illustrated in Figure 64. Figure 65 shows the corresponding real and detected miss distance curves after this new noise curve is added to Path One. Comparing Figures 34 and 65, it can be seen that this constant angle error does not affect the miss distance detection nor the threshold curves.

In another case, the same noise curve is added to Path Two. Figure 66 shows the corresponding miss distance error curve. Again, comparing Figure 48 and 66, it can also be seen that a constant angle error does not affect the miss distance error curve.

IV. CONCLUSIONS

A computer program has been developed to simulate the Enhanced TCAS II System tracking a single target. There are four basic components in this model, namely, the target path, noise, the alpha beta filter and the threat detecting algorithm. The implementation of each of these four components was discussed in this report. It is noted that the aircraft use here for demonstration purposes is a Boeing 737 with the TCAS II antenna mounted on top of the fuselage, about 35 ft. from the nose. The same procedure used here can be followed to simulate a different aircraft or to study the case when the TCAS antenna is mounted on the bottom of the fuselage. It is important to keep in mind that the antenna location plays a very important role on the computer model of the aircraft.

As stated at the introduction, the performance of the system is negatively affected by interference, hardware-related errors, thermal noise, stability of the inertial navigation system, distortion of the antenna patterns by own aircraft (also referred to as structural scattering), etc. In this study, all these sources of errors were separated into two groups, namely, the errors due to structural scattering in one group and all the other sources of errors in another group. The latter group was modeled as a Gaussian noise source with zero mean and a variance which was obtained from the error budget presented in [2]. Thus, a careful study can be done of the errors introduced by the structural scattering alone. A large number of results were presented of the bearing errors as a function of azimuth for several elevation angles. Results were shown for a system with 8

and 64 beam positions, and as expected, the errors are smaller when 64 beam positions are used instead of 8. It was also shown that there is a large increase in errors for negative angles of elevation, i.e., for observation points below the horizon, when only a top-mounted antenna is used.

In order to demonstrate the capabilities of the computer model described here, two encounters were studied in detail. In one encounter, the target approaches the TCAS II protected aircraft from the front (Path One); while in the second encounter (Path Two), the target approaches the TCAS II aircraft from behind. It was observed that structural scattering plays an important role on the accuracy of the system when the target approaches from behind which is expected due to strong scattering by the tail of the aircraft. On the other hand, when the target approaches the TCAS II protected aircraft on Path One, the noise seems to affect the accuracy of the system more than structural scattering.

An important feature of the computer simulation is that an encounter of the TCAS II protected aircraft with the target can be depicted on a color graphics display where the coordinate system is fixed with the TCAS II aircraft. As the target approaches the TCAS II airplane, the calculated and true path followed by the target is shown. Furthermore, the true and calculated velocity of the target, the time to CPA and the miss distance at CPA are also displayed. Thus, one can immediately evaluate the performance of the TCAS II system.

In addition to the path followed by the target, two threshold curves (one on each side of the target's path) are also plotted. Thus,

at a certain time before CPA, e.g., 30 secs, if the target is within the threshold curves, there is danger of collision and a decision can be made so that the target (relative to the TCAS II aircraft) takes an escape path. Results were shown where the target takes an escape path of "6 secs. rollover to 45°"; however, the roll of the aircraft as it changes bearing is not taken into account at the present time. Thus, the results are probably better than what actually happens when only a top-mounted antenna is used. In the future, the roll of the aircraft will be taken into account in order to have a more realistic simulation.

As a final remark, the computer simulation described here can be used to test the performance of the TCAS II antenna mounted on the fuselage of an aircraft as it tracks a single target. For example, several threshold equations can be tested to find the one that gives best results.

APPENDIX I

THE COLOR CODE FOR THE GKS DISPLAY

(1) ++++++++++ The actual target location when its elevation angle is between 0° and 30°.

(2) . . . . . The actual target location when its elevation angle is greater than 30°.

(3) XXXXXXXXXX The detected target location when the alarm is not turned on.

(4) XXXXXXXXXX The detected target location when the alarm is turned on.

(5) XXXXXXXXXX The detected target location when the alarm could have been turned off if the protected aircraft would have taken the 6 second rollover to 45° escape path. It is emphasized that the protected aircraft did not actually change its original path.

(6) OOOOOOOOOO Same as (3) but for the target elevation angle greater than 30°.

(7) OOOOOOOOOO Same as (4) but for the target elevation angle greater than 30°.

(8) OOOOOOOOOO Same as (5) but for the target elevation angle greater than 30°.

(9) ********** The detected miss distance curve.

(10) ———————— The threshold curve.

(11) —·—·—·—·— The 10 second rollover to 45° path.

(12) - - - - - - - - - - - - The 6 second rollover to 30° path.

(13) ———————— The 6 second rollover to 45° path.

REFERENCES

[1] W.D. Burnside, J.J. Kim, B. Grandchamp, R.G. Rojas and P. Law, "Airborne Antenna Radiation Pattern Code User's Manual," Report 716199-4, The Ohio State University ElectroScience Laboratory; prepared under Grant No. NSG-1498 for NASA - Langley Research Center, September 1985.

[2] A.I. Sinsky, R.J. Tier, "System Angle Accuracy Prediction," Report No. BCD-TN-82-035, The Bendix Corporation, Communications Division; prepared under Contract No. DTFA01-82-C-10019 for the U.S. Department of Transportation, FAA, July 1982.

[3] A.I. Sinsky, "Miss Distance Prediction Algorithm," Report No. BCD-TN-84-004, The Bendix Corporation, Communications Division; prepared under Contract No. DTFA-1-82-C-10019 for the U.S. Department of Transportation, FAA, February 1984.

[4] "Enhanced TCAS II System Summary," Report No. BCD-TR-098, The Bendix Corporation, Communications Division; prepared under Contract No. DTFA01-82-C-10019 for the U.S. Department of Transportation, FAA, April 1984.

[5] A.I. Sinsky, "Alpha-Beta Tracking Errors for Orbiting Targets," Report No. BCD-TN-81-033, The Bendix Corporation, Communications Division; prepared under Contract No. DTFA01-81-C-10041 for the U.S. Department of Transportation, FAA, June 1981.

[6] R.G. Rojas, W.D. Burnside, P. Law and B. Grandchamp, "Simulation of the Enhanced Traffic Alert and Collision Avoidance System (TCAS II)," Semi-Annual Report 716199-3, The Ohio State University ElectroScience Laboratory, prepared under Grant No. NSG 1498 for NASA - Langley Research Center, September 1985.

[7] P. Law, W.D. Burnside and R.G. Rojas, "A Study of a Collision Avoidance System Mounted on a Curved Ground Plane," Semi-Annual Report 716199-8, prepared under Grant No. NSG 1498 for NASA - Langley Research Center, March 1986.

[8] B.J. Grandchamp, "A Study of the TCAS II Collision Avoidance System Mounted on a Boeing 737 Aircraft," M.Sc. thesis, The Ohio State University, Department of Electrical Engineering, Columbus, Ohio, 1985.

[9] "Enhanced TCAS II," Bimonthly Review, The Bendix Corporation, Communications Division; prepared under Contract No. DTFA01-82-C-10019 for Federal Aviation Administration, February 2, 1984.

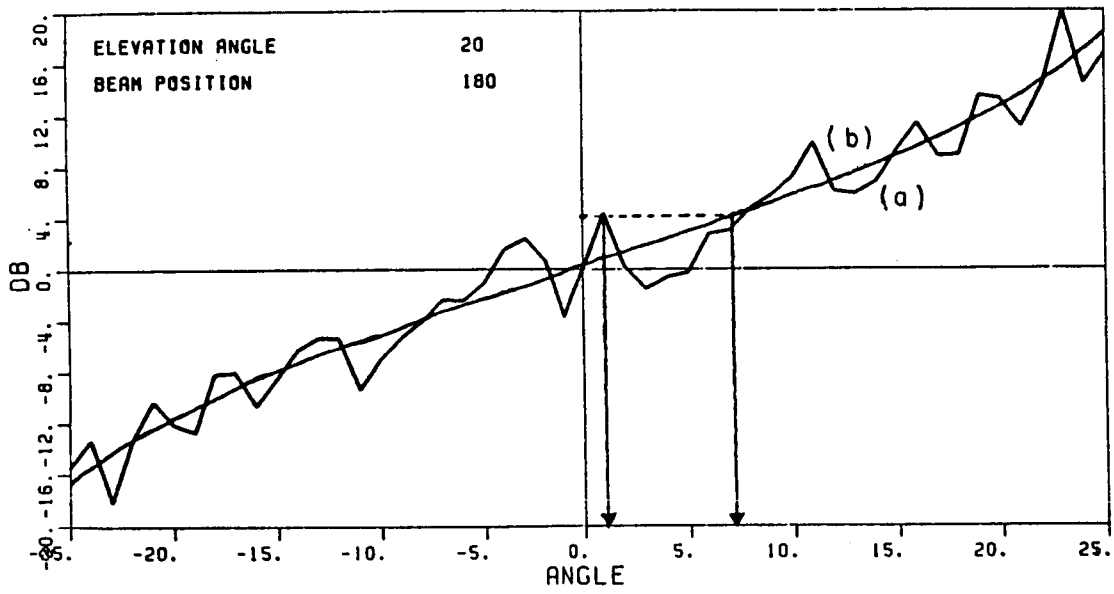

Frequency = 1.06 GHz

(a) Received monopulse characteristic curve
(b) Lookup monopulse characteristic curve

Figure 1. Received and lookup monopulse characteristic curves.

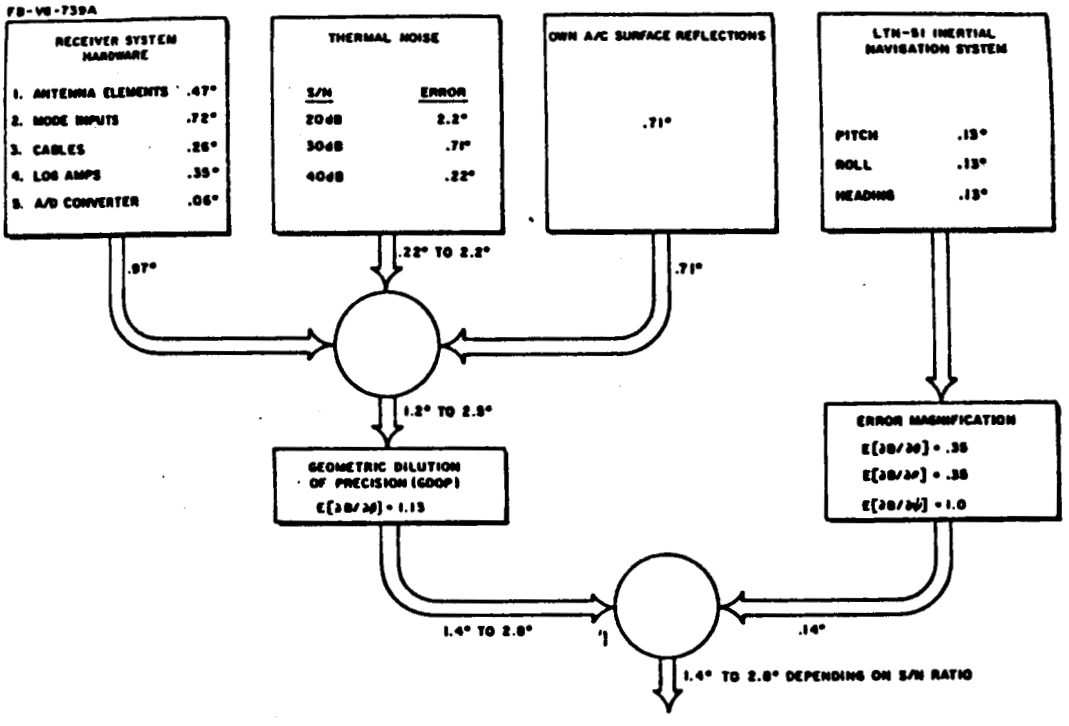

Figure 2. Absolute angle error summary, obtained from Reference [2].

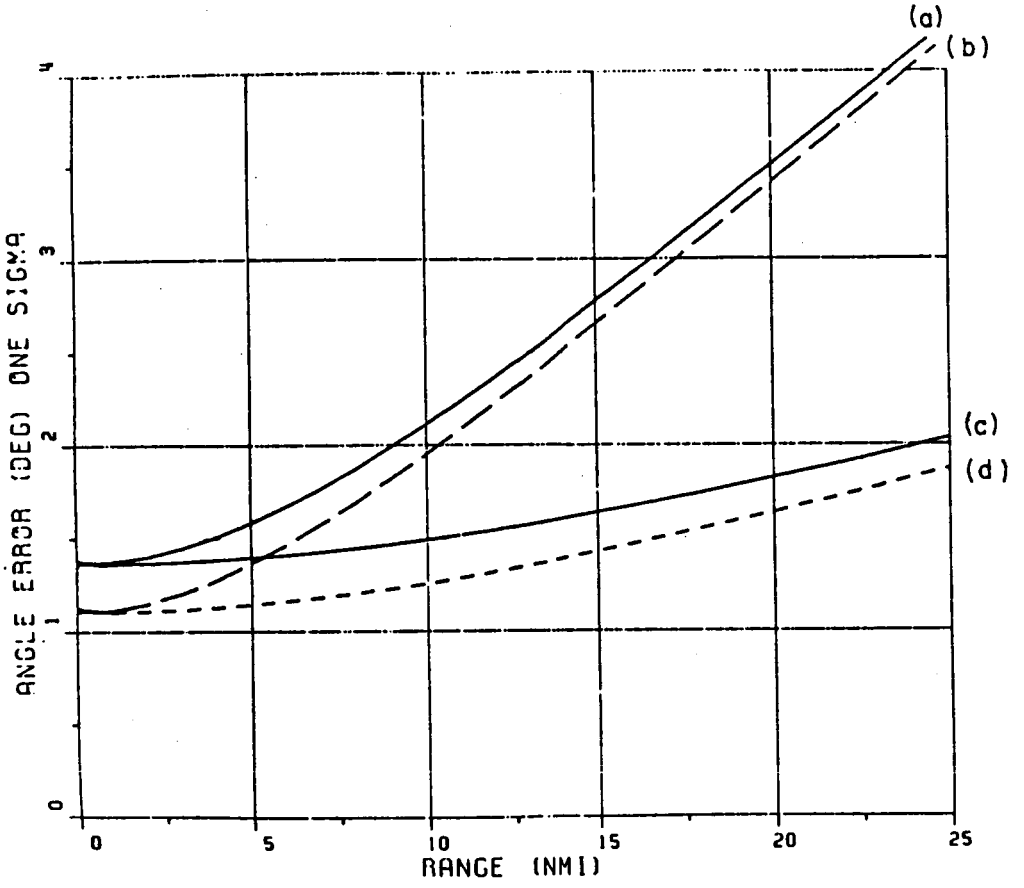

(a) Transponder power of 18.5 dBw (Equation (2))
(b) Transponder power of 18.5 dBw but excluding scattering errors (Equation (3))
(c) Transponder power of 27 dBw (Equation (2))
(d) Transponder power of 27 dBw but excluding scattering errors (Equation (3)).

Figure 3. Absolute angle accuracy, obtained from Reference [2].

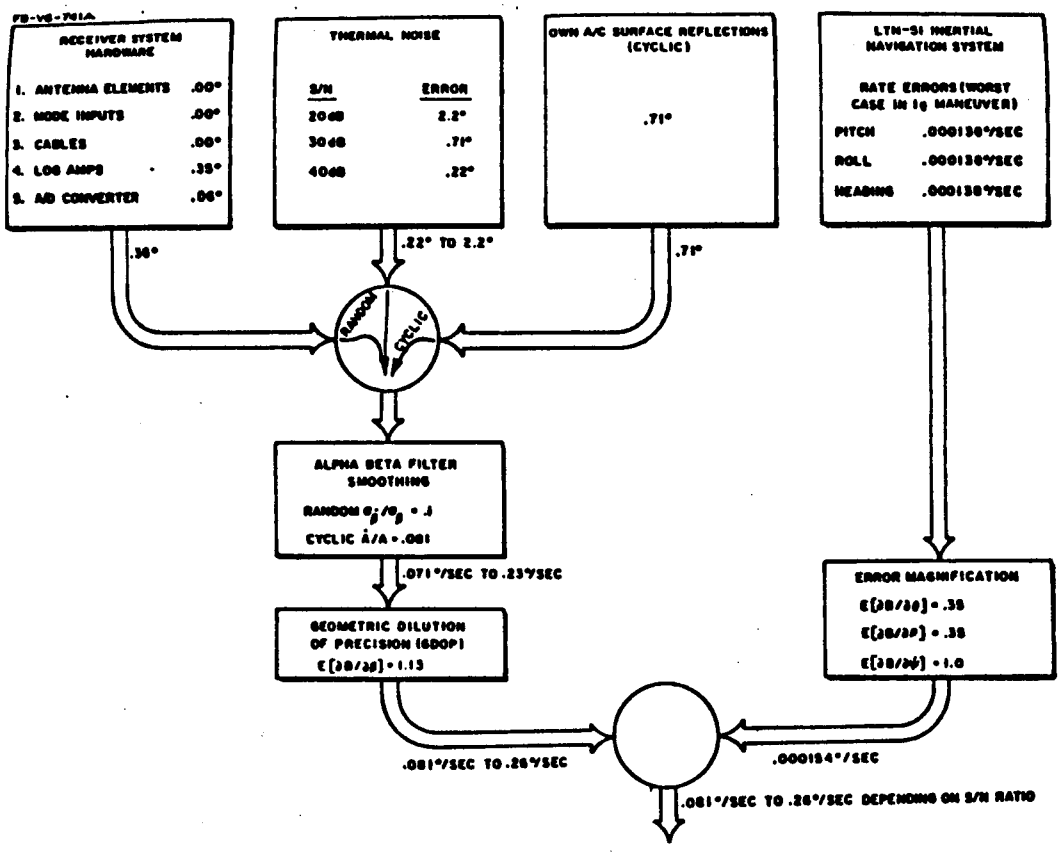

Figure 4. Angle rate error summary, obtained from Reference [2].

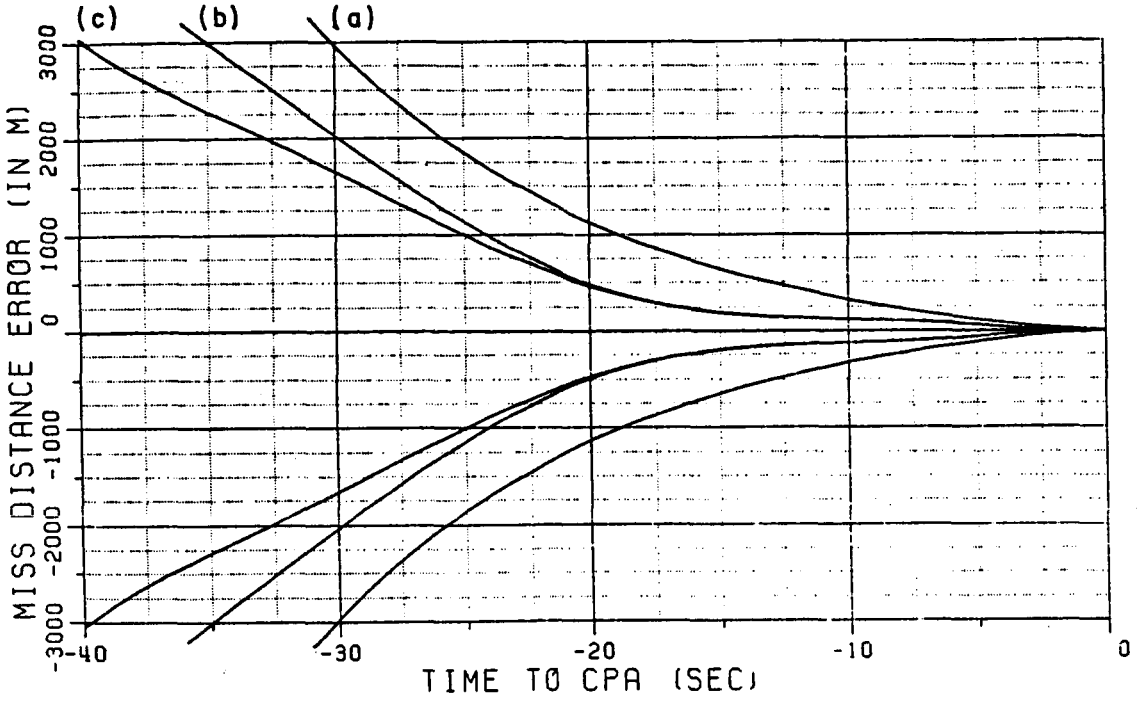

(a) 6 seconds rollover to 45°
(b) 10 seconds rollover to 45°
(c) 6 seconds rollover to 30°

Figure 5. Escape curves.

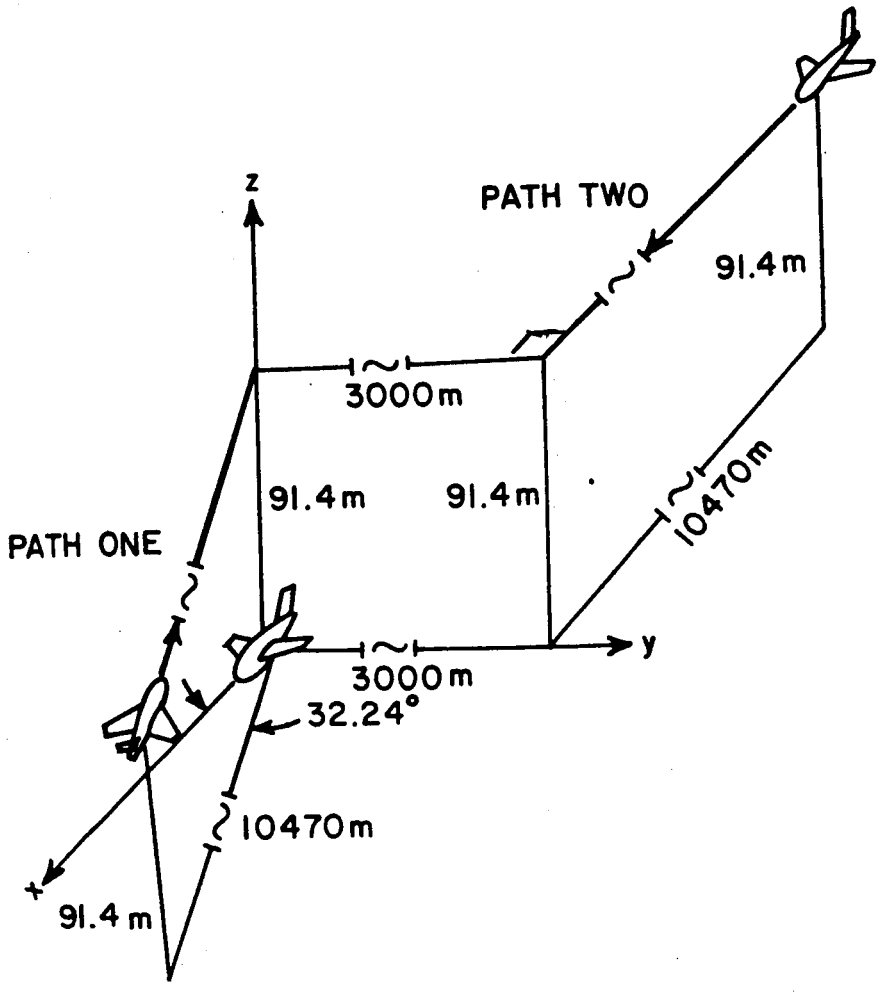

Equation for Path One: y=tan(32.24° x), z=91.4 m
starting at x=8857 m, speed=174.5 m/s

Equation for Path Two: y=3000m, z=91.4 m
starting at x=-10470m, speed=174.5 m/s

Figure 6. The simulated flight paths.

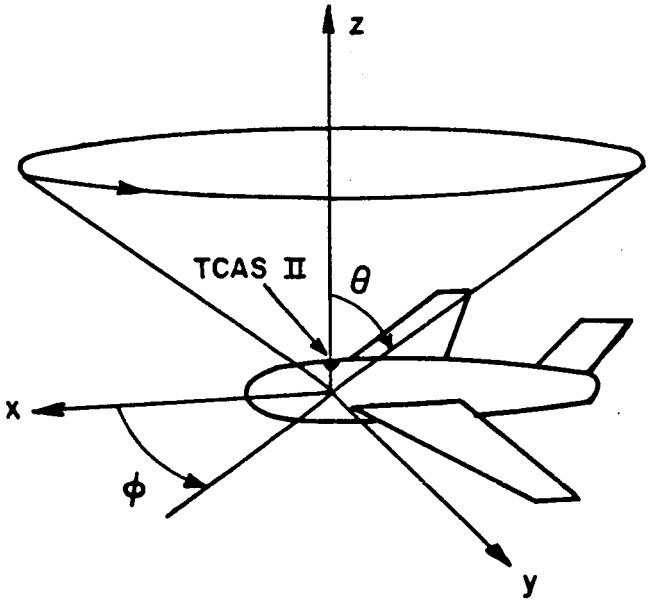

Elevation angle=90-θ
Azimuth angle=ϕ

Figure 7. The coordinate system of the TCAS II system used in this report.

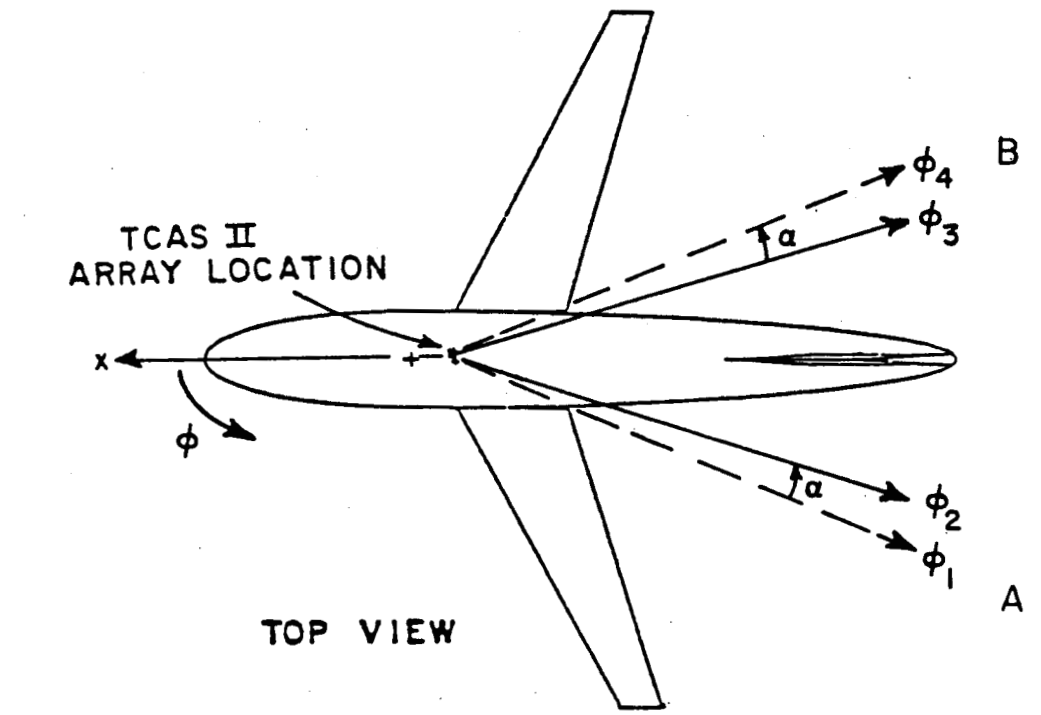

When the target is at A, the bearing error is $\phi_2-\phi_1=\alpha$.
When the target is B, the bearing error is $\phi_3-\phi_4=-\alpha$.

Figure 8. Convention used to measure bearing error of the TCAS II equipped Boeing 737.

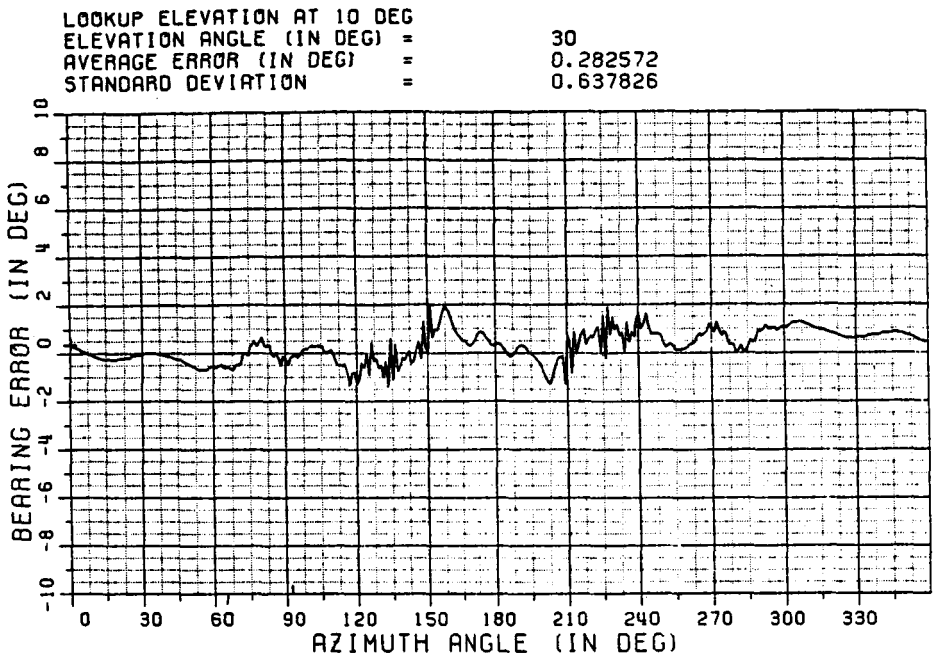

(a) Bearing errors obtained with 64 beam positions

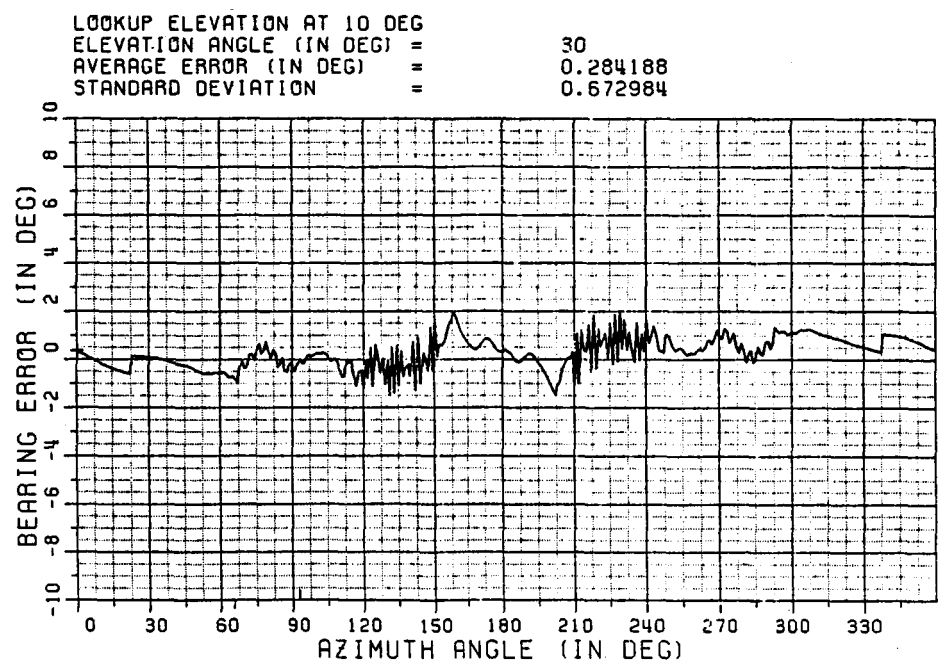

(b) Bearing errors obtained by 8 beam positions

Figure 9. Bearing errors as a function of azimuth angles.

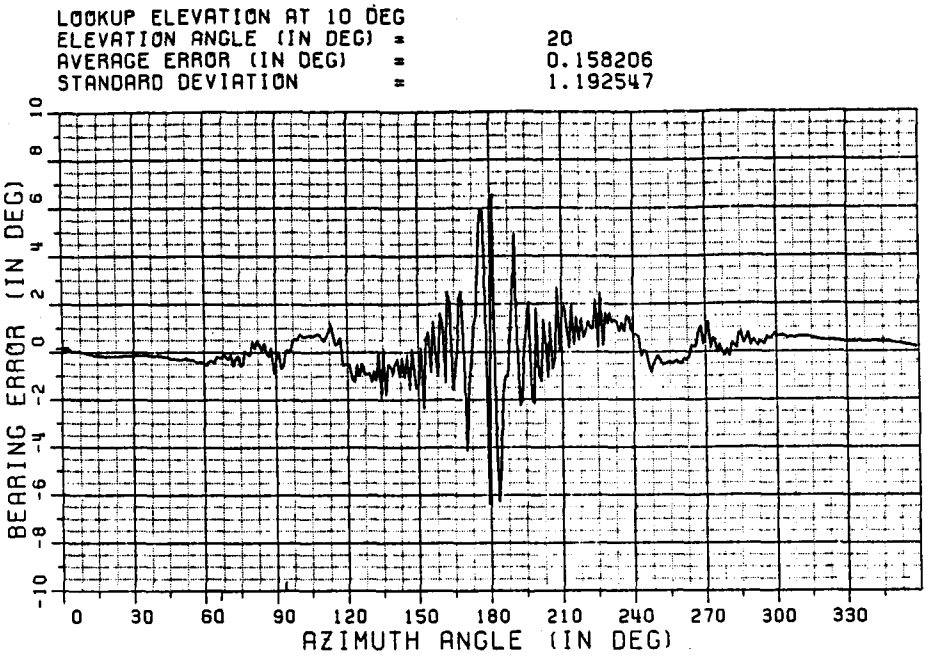

(a) Bearing errors obtained with 64 beam positions

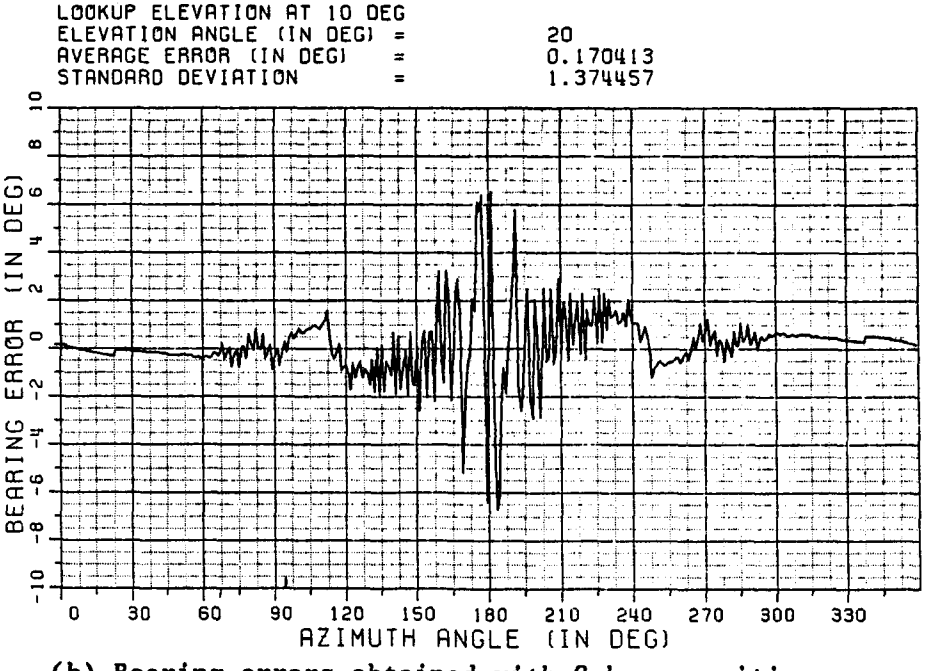

(b) Bearing errors obtained with 8 beam positions

Figure 10. Bearing errors as a function of azimuth angles.

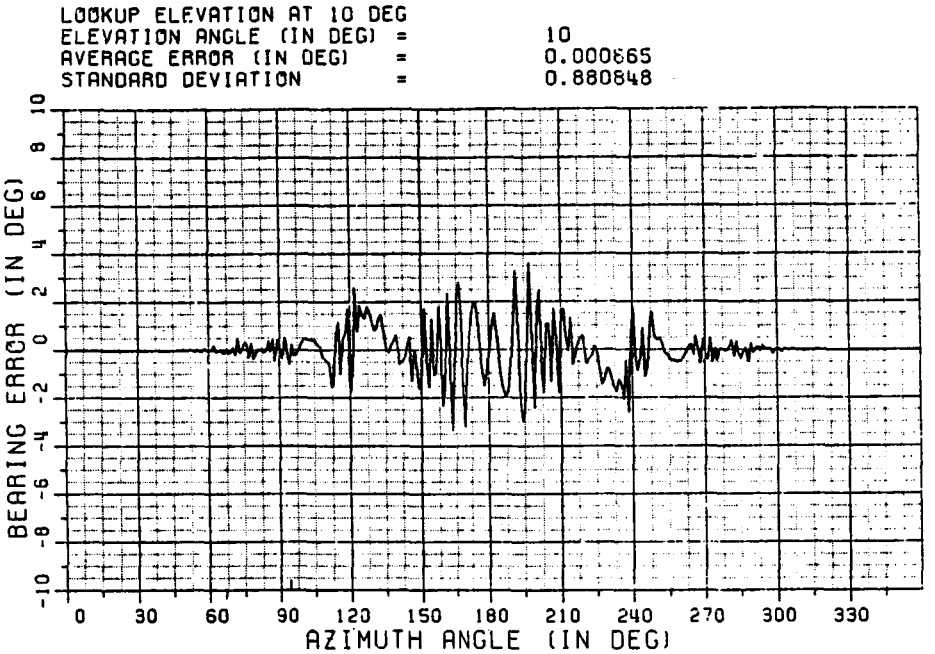

(a) Bearing errors obtained with 64 beam positions

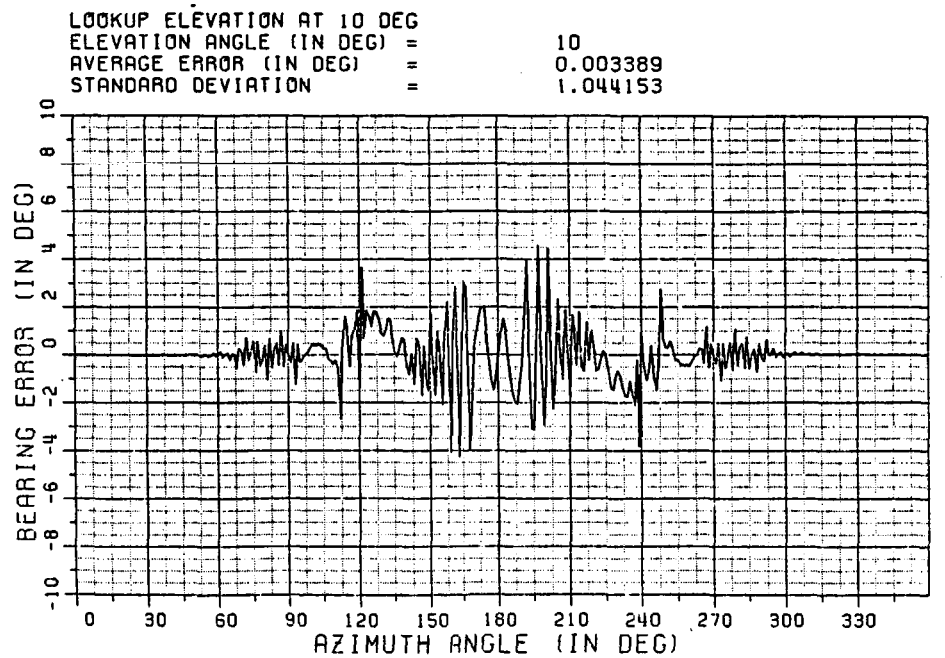

(b) Bearing errors obtained with 8 beam positions

Figure 11. Bearing errors as a function of azimuth angles.

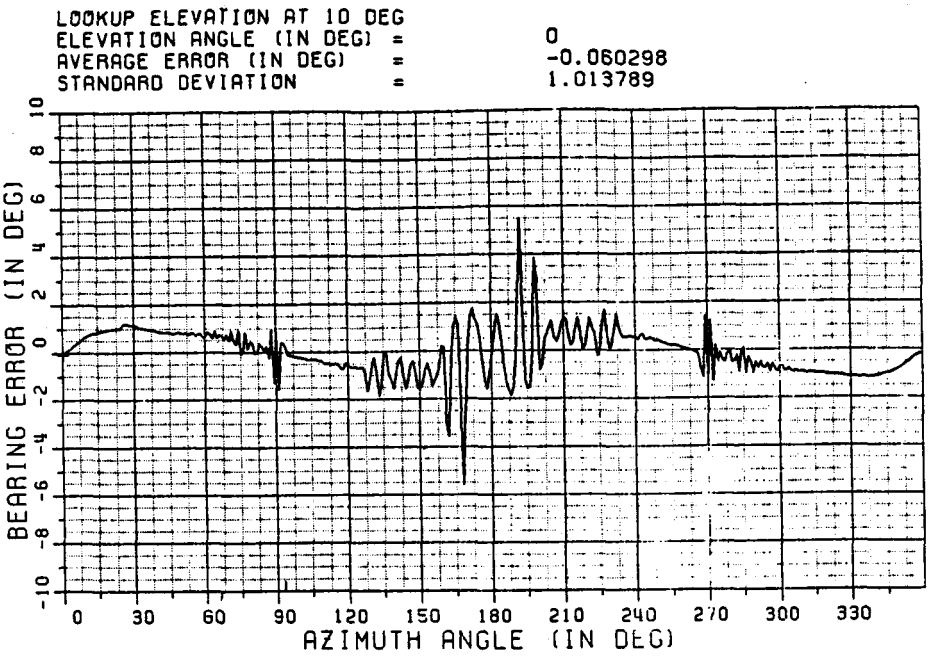

(a) Bearing errors obtained with 64 beam positions

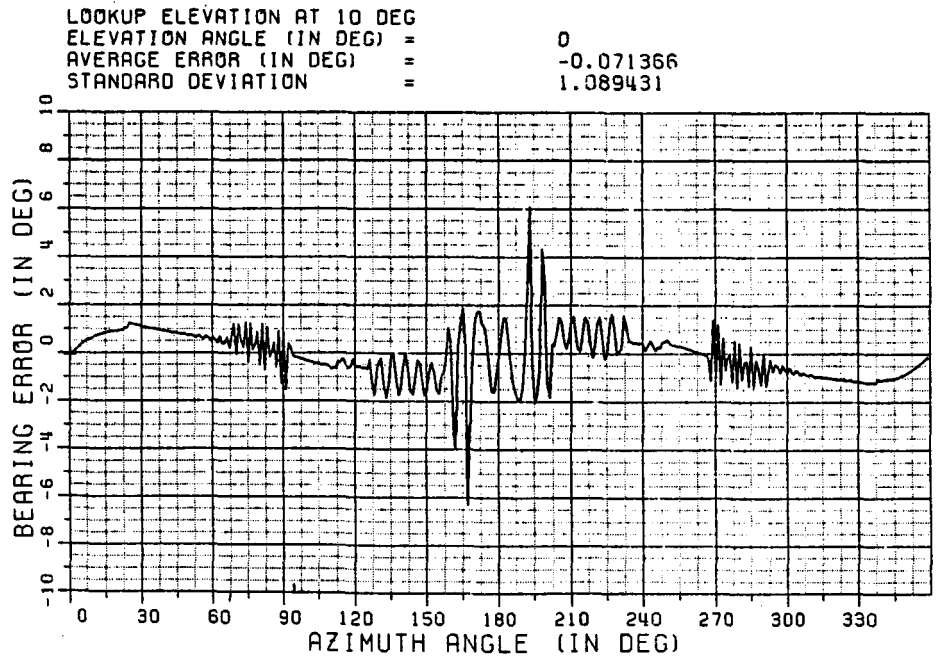

(b) Bearing errors obtained with 8 beam positions

Figure 12. Bearing errors as a function of azimuth angles.

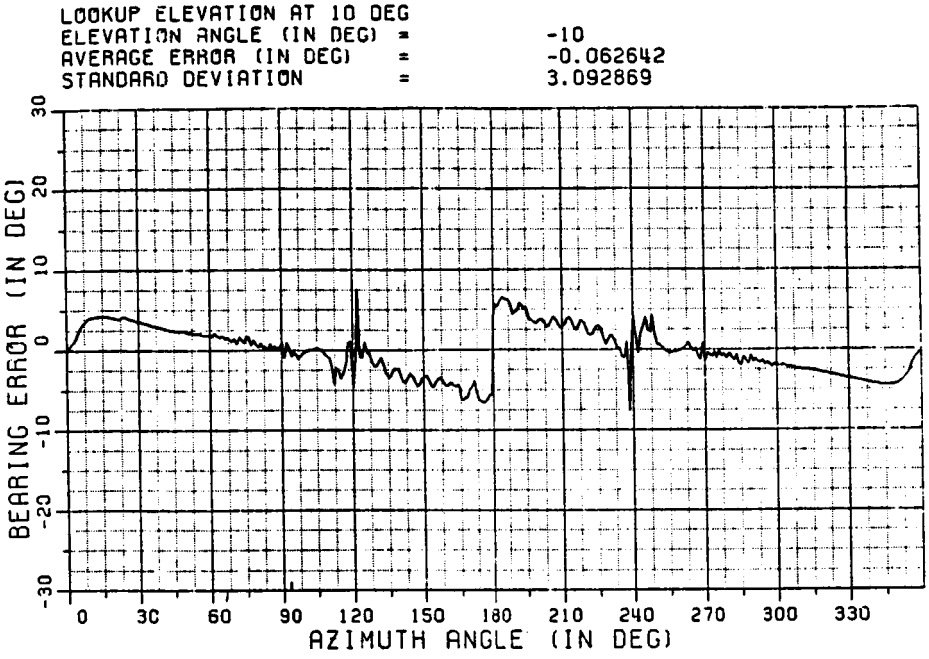

(a) Bearing errors obtained with 64 beam positions

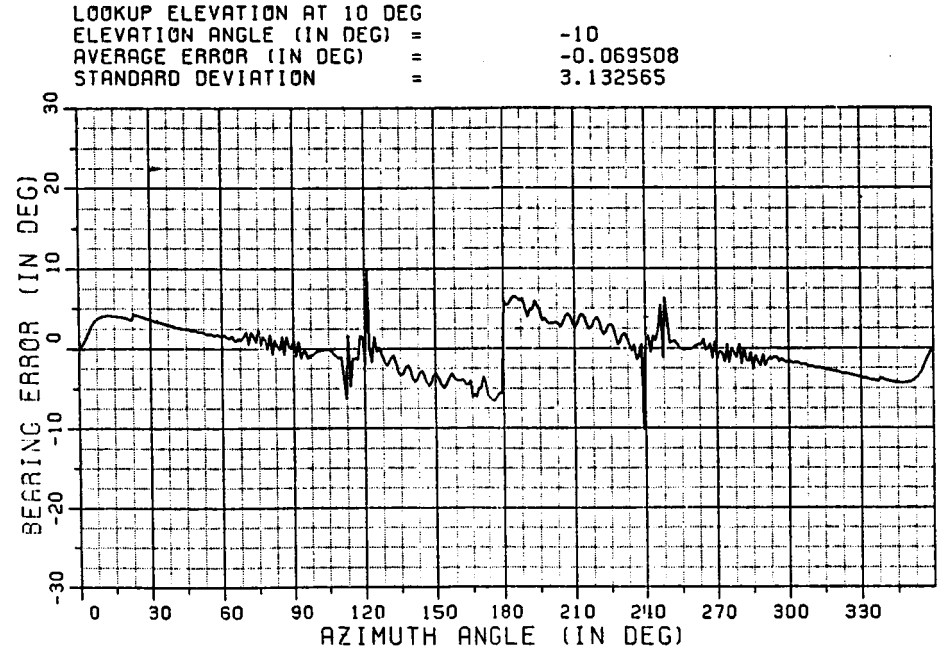

(b) Bearing errors obtained with 8 beam positions

Figure 13. Bearing errors as a function of azimuth angles.

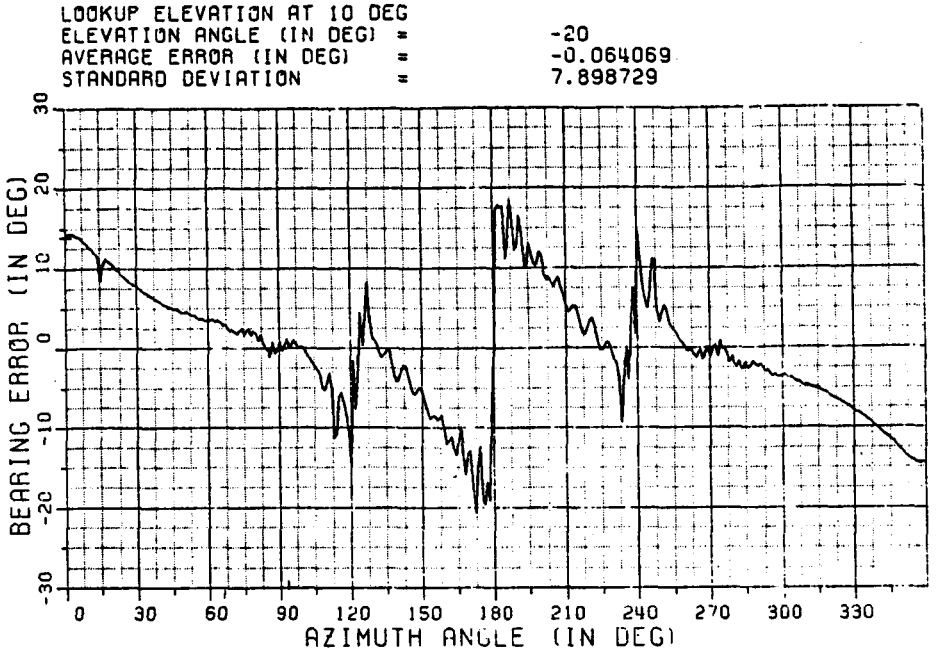

(a) Bearing errors obtained with 64 beam positions

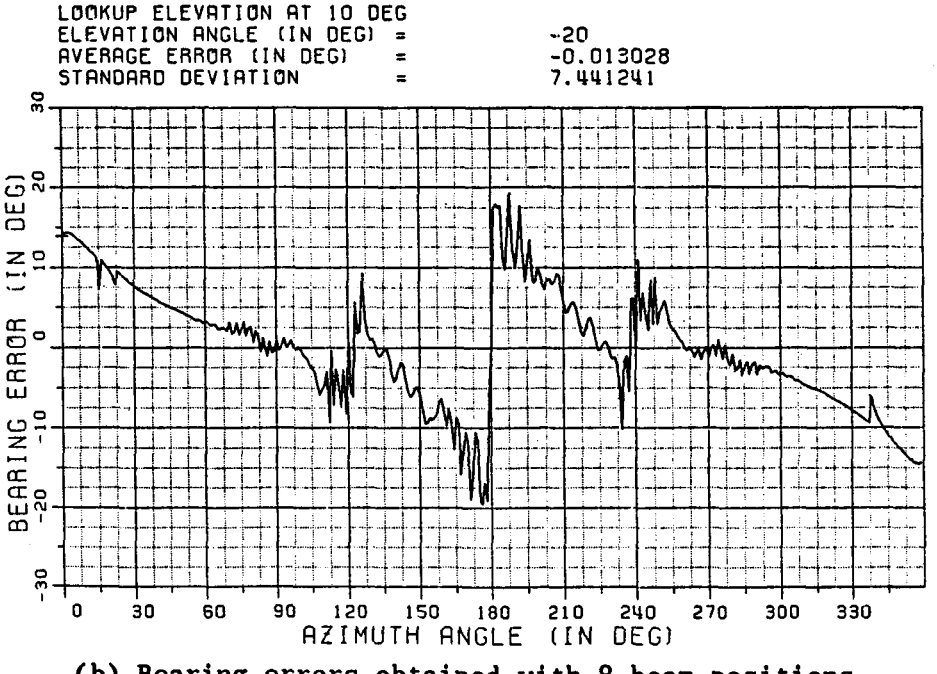

(b) Bearing errors obtained with 8 beam positions

Figure 14. Bearing errors as a function of azimuth angles.

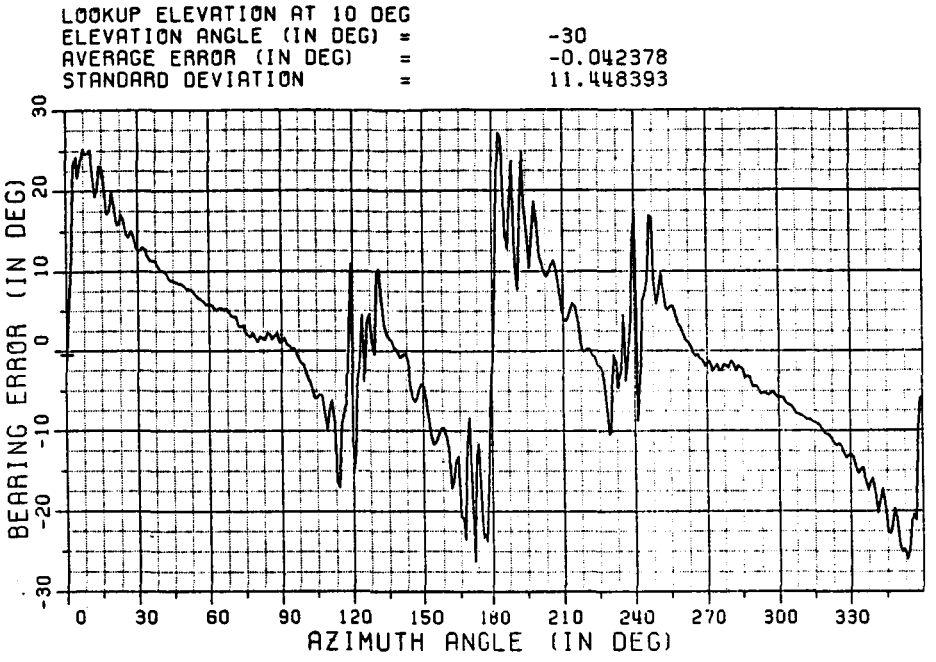

(a) Bearing errors obtained with 64 beam positions

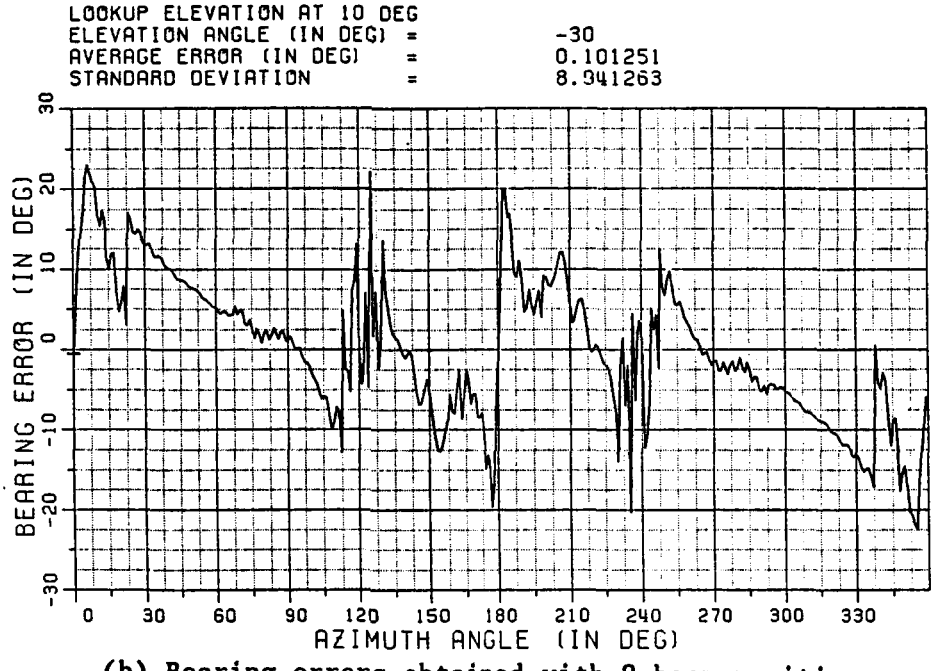

(b) Bearing errors obtained with 8 beam positions

Figure 15. Bearing errors as a function of azimuth angles.

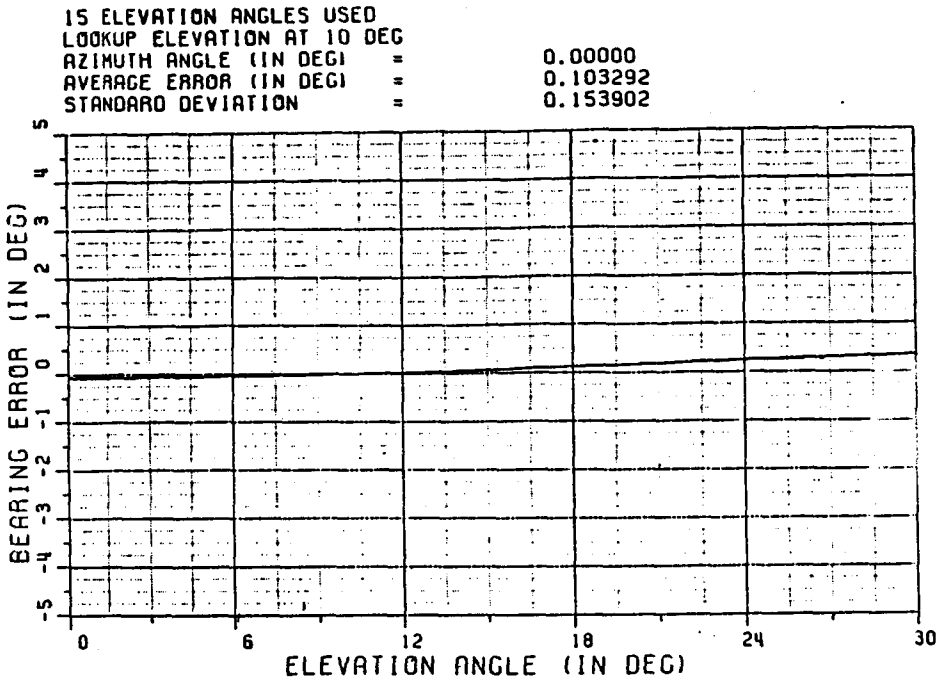

Figure 16. Bearing errors as a function of elevation angles (obtained by using 8 beam positions).

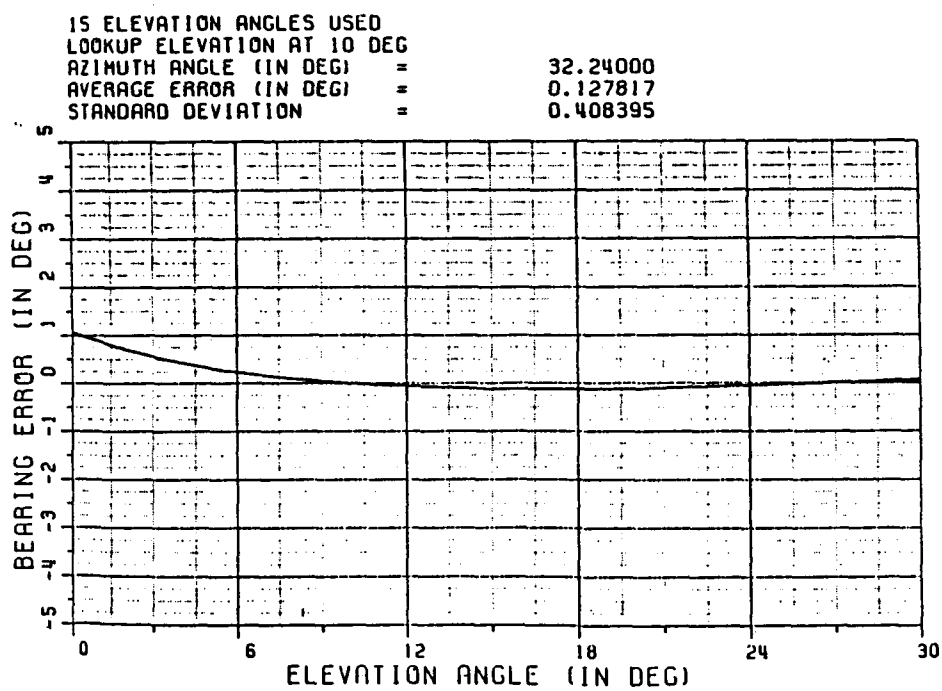

Figure 17. Bearing errors as a function of elevation angles (obtained by using 8 beam positions).

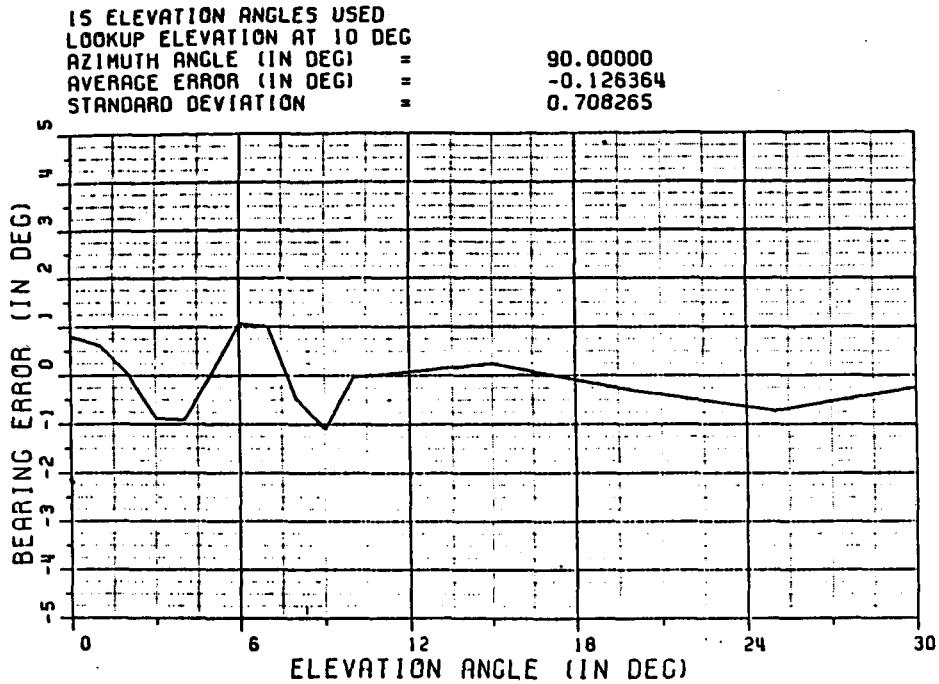

Figure 18. Bearing errors as a function of elevation angles (obtained by using 8 beam positions).

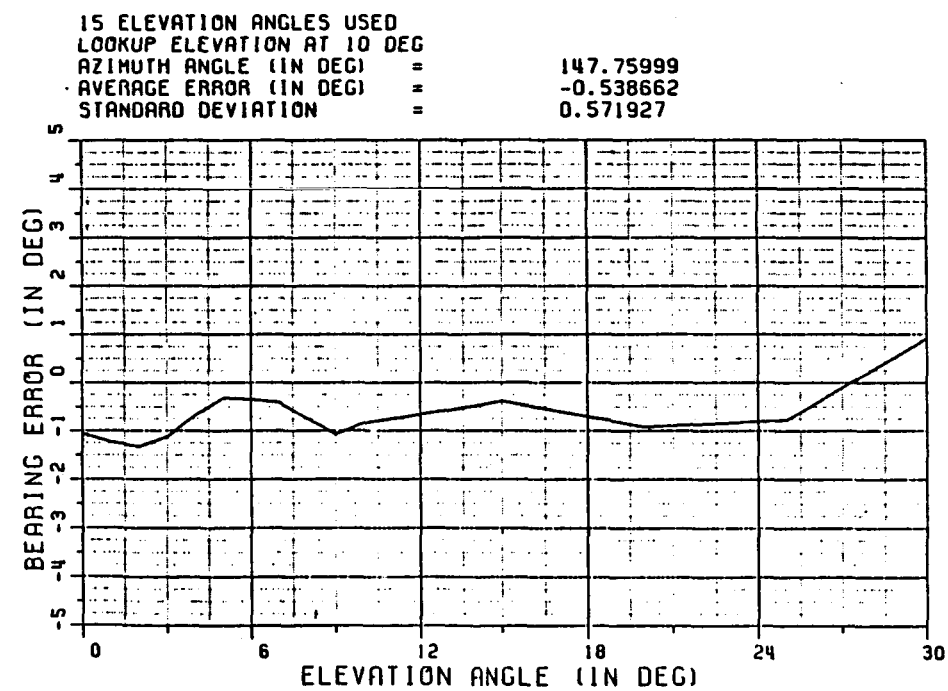

Figure 19. Bearing errors as a function of elevation angles (obtained by using 8 beam positions).

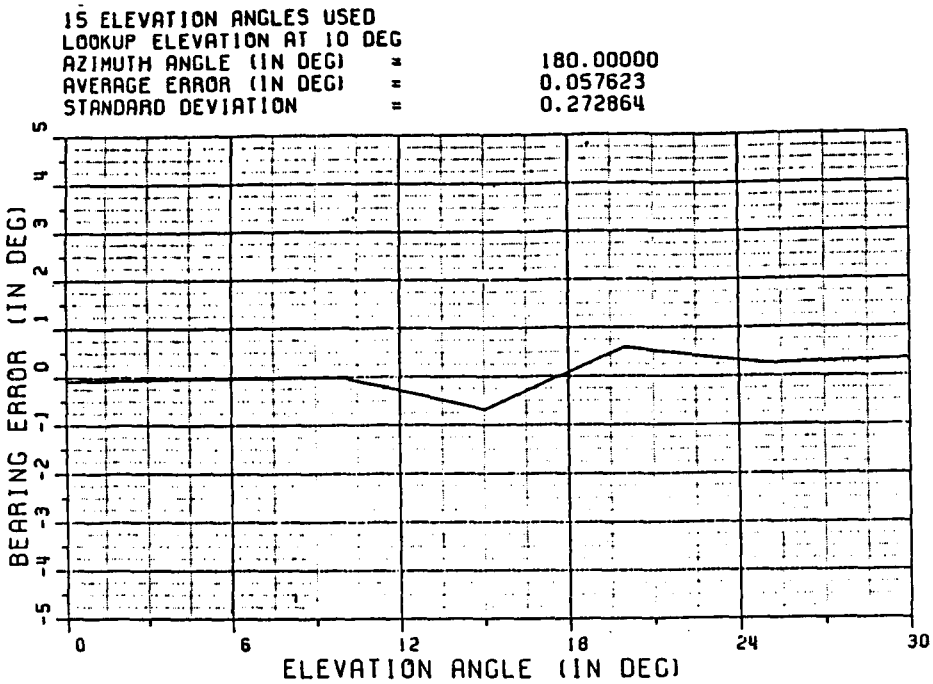

Figure 20. Bearing errors as a function of elevation angles (obtained by using 8 beam positions).

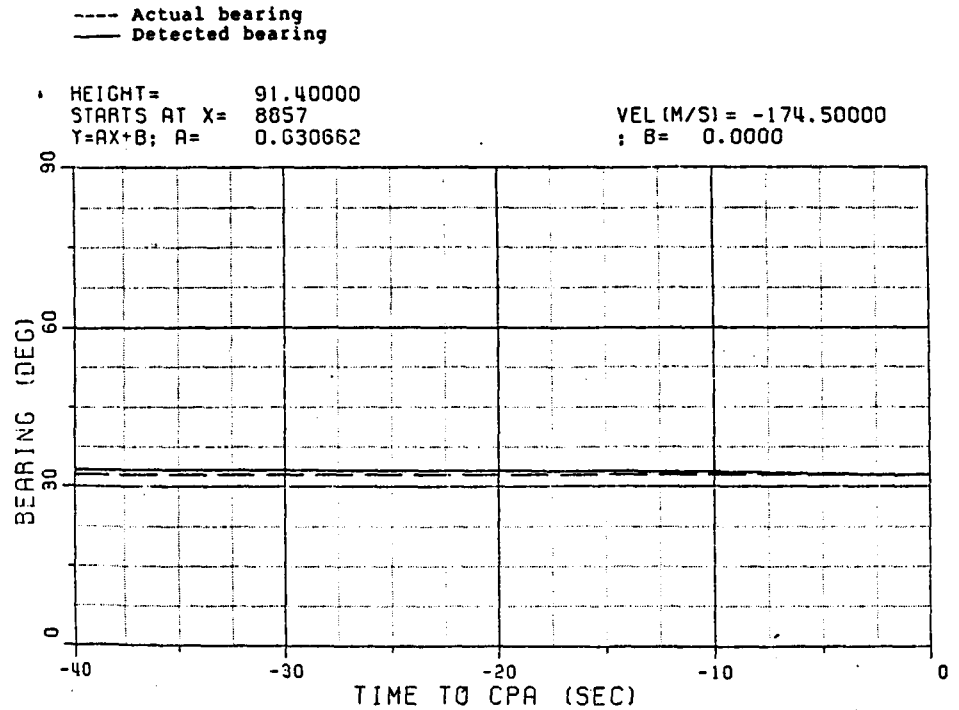

Figure 21. Detected and actual target bearing on Path One with only scattering effects.

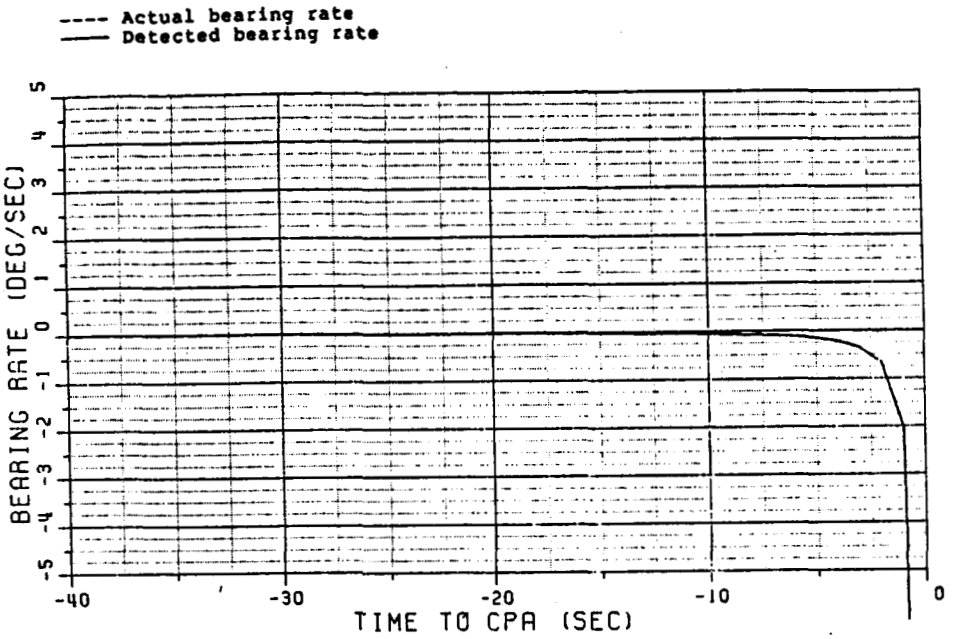

Figure 22. Bearing rate curve on Path One with only scattering effects.

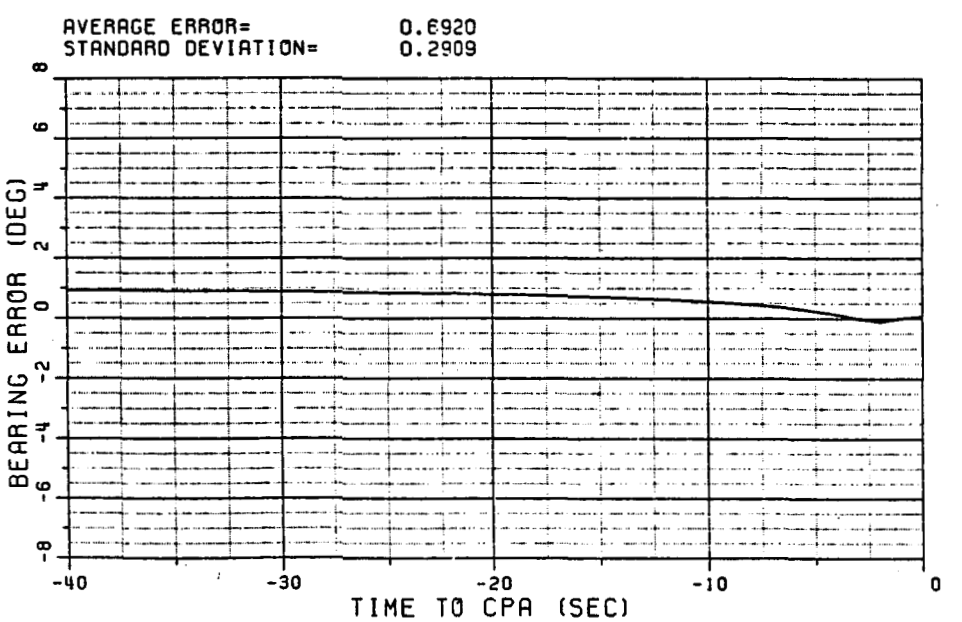

Figure 23. Bearing errors corresponding to Figure 21.

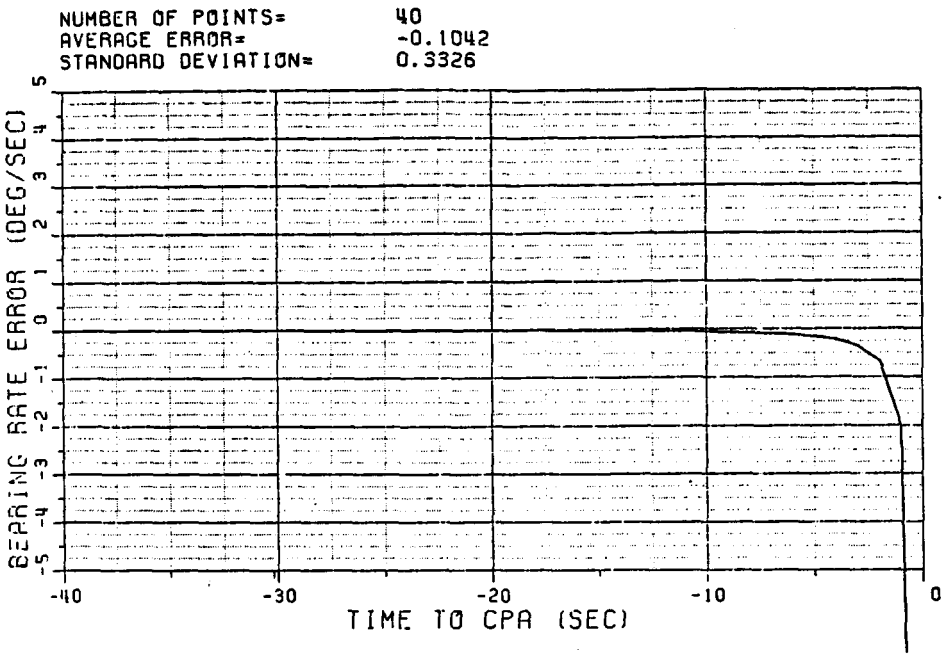

Figure 24. Bearing rate errors corresponding to Figures 21.

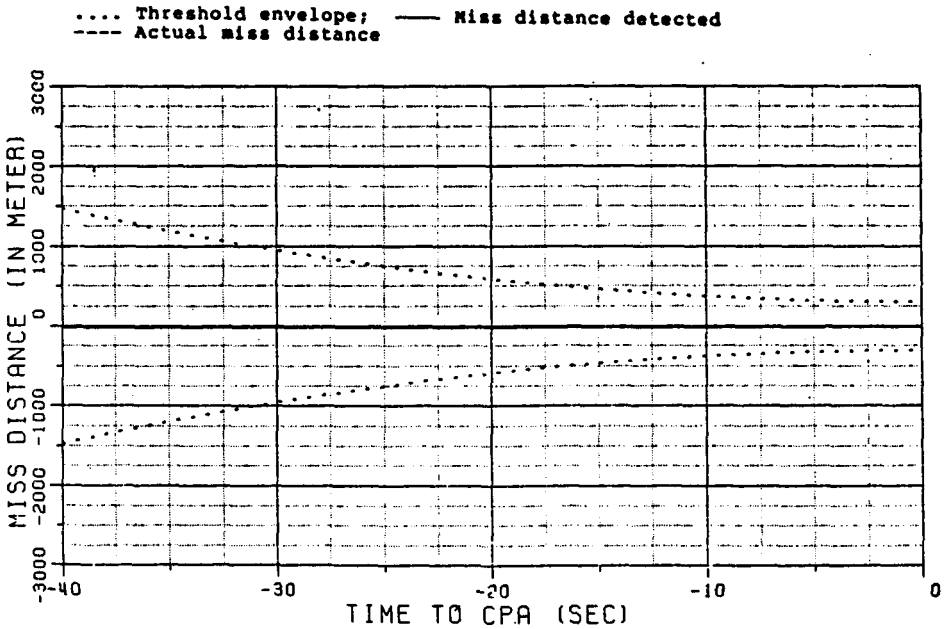

Figure 25. Threshold and miss distance curves on Path One with only scattering effects.

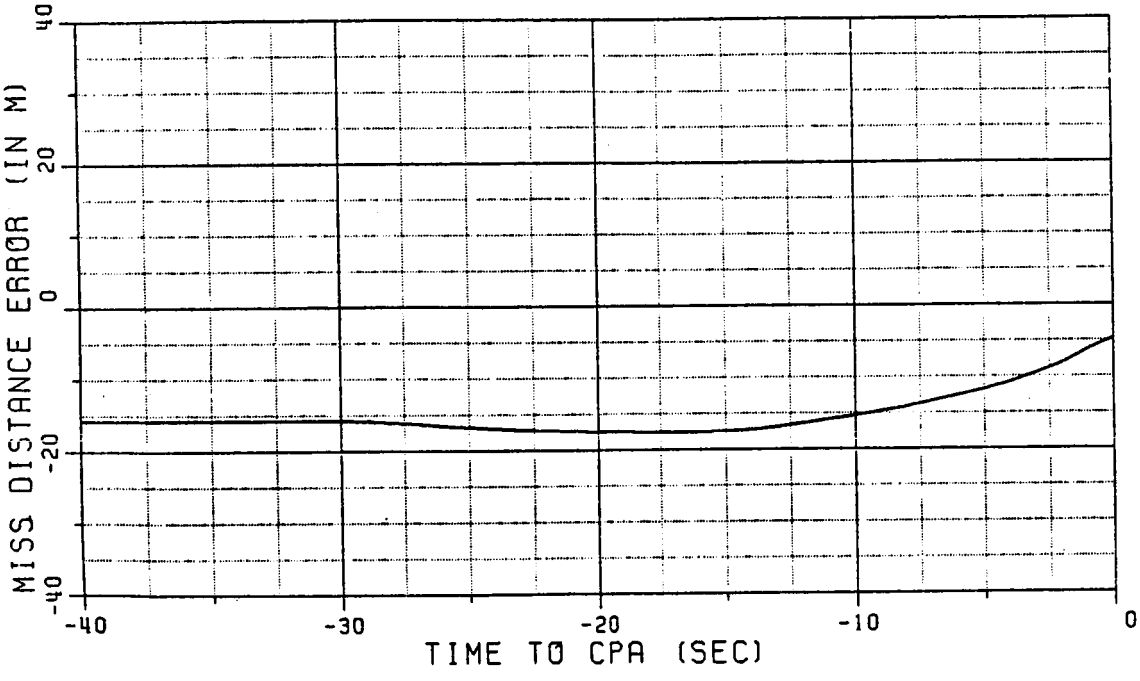

Figure 26. Miss distance error curve on Path One with only scattering effects.

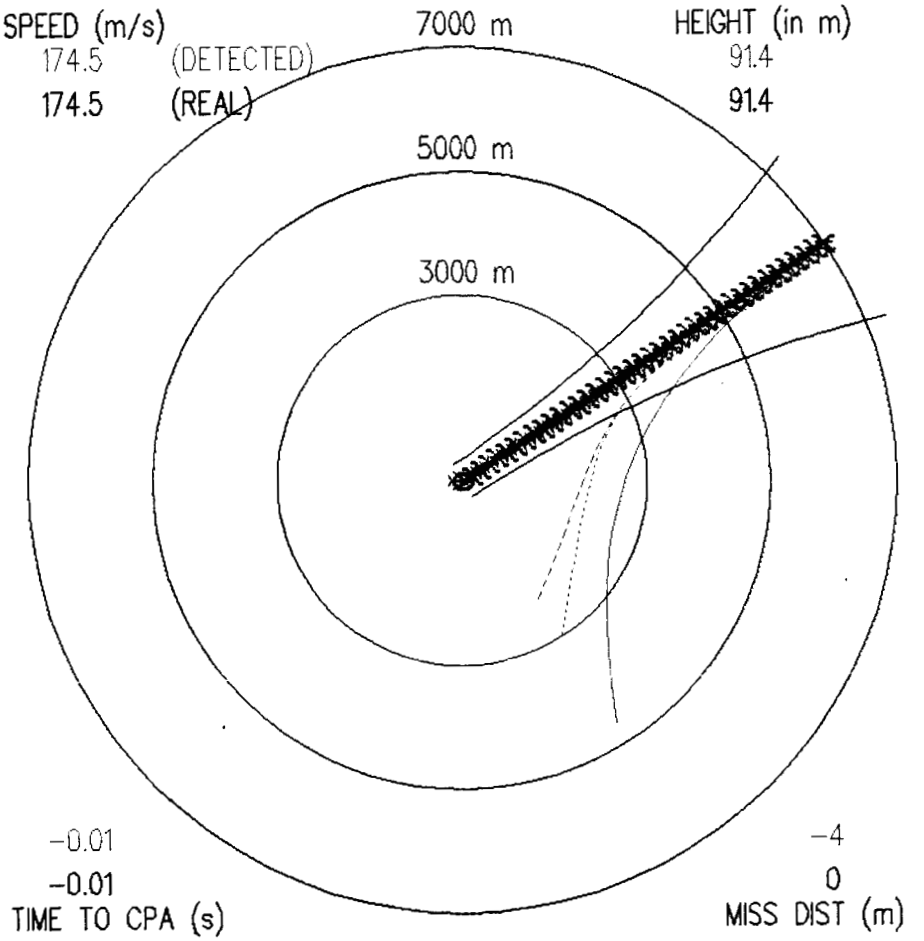

Figure 27. The graphic display of Path One with only scattering effects.

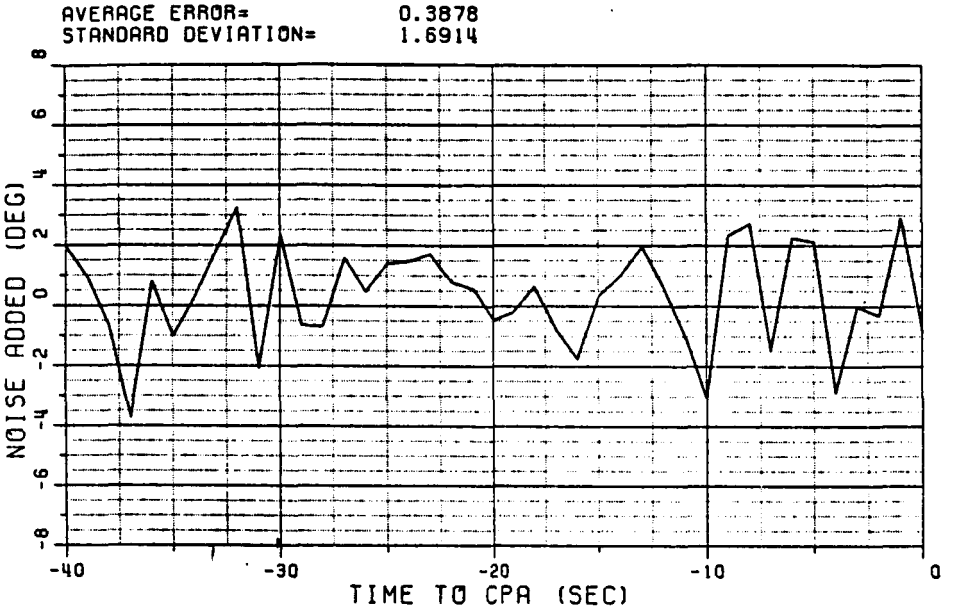

Figure 28. Noise added on Paths One and Two.

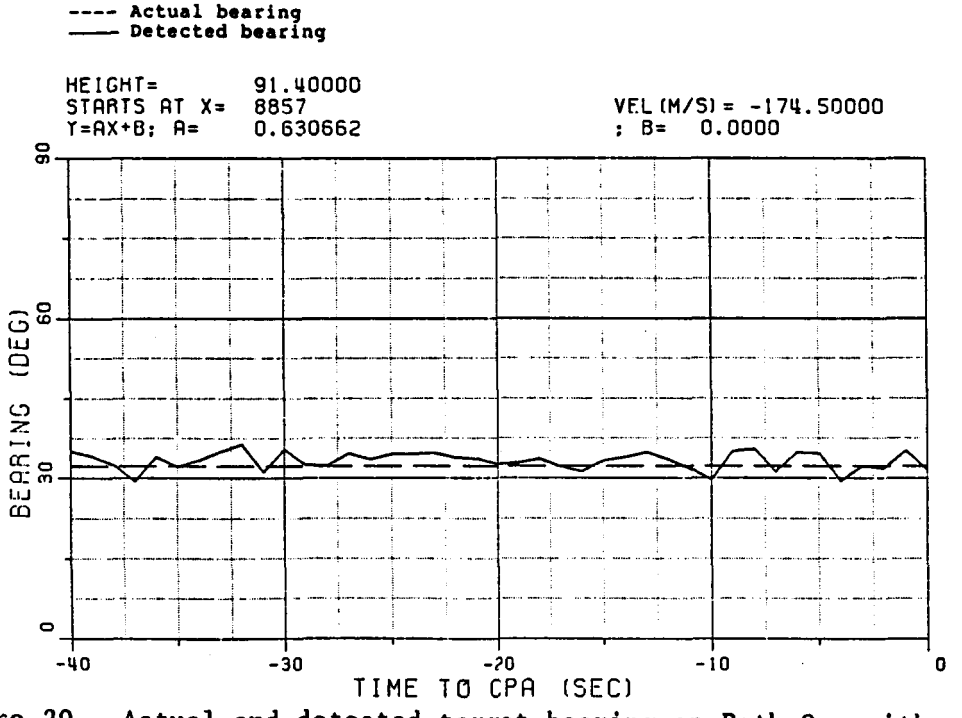

Figure 29. Actual and detected target bearing on Path One with noise and scattering effects.

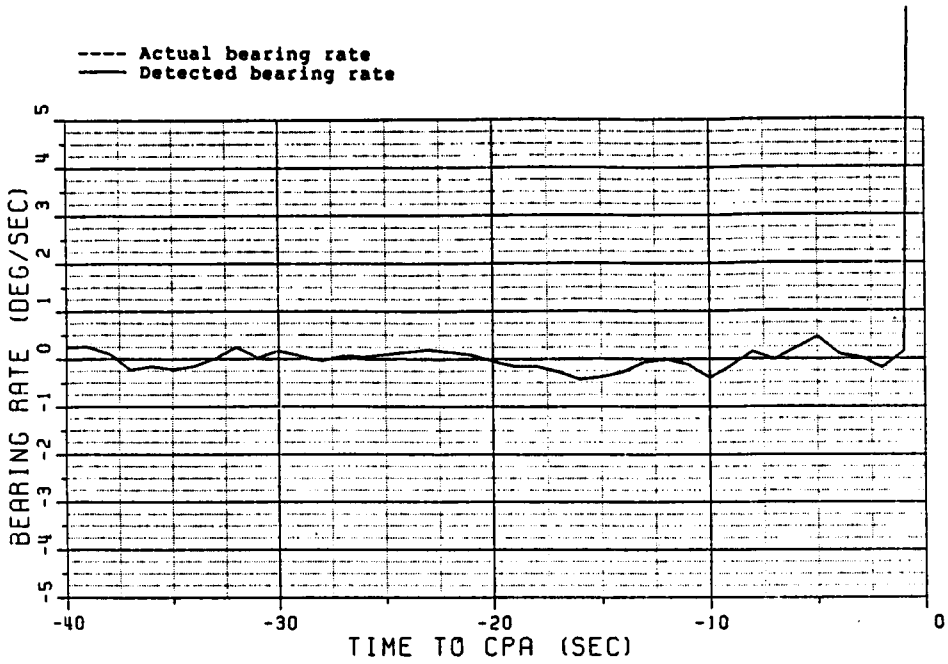

Figure 30. Bearing rate curve on Path One with noise and scattering effects.

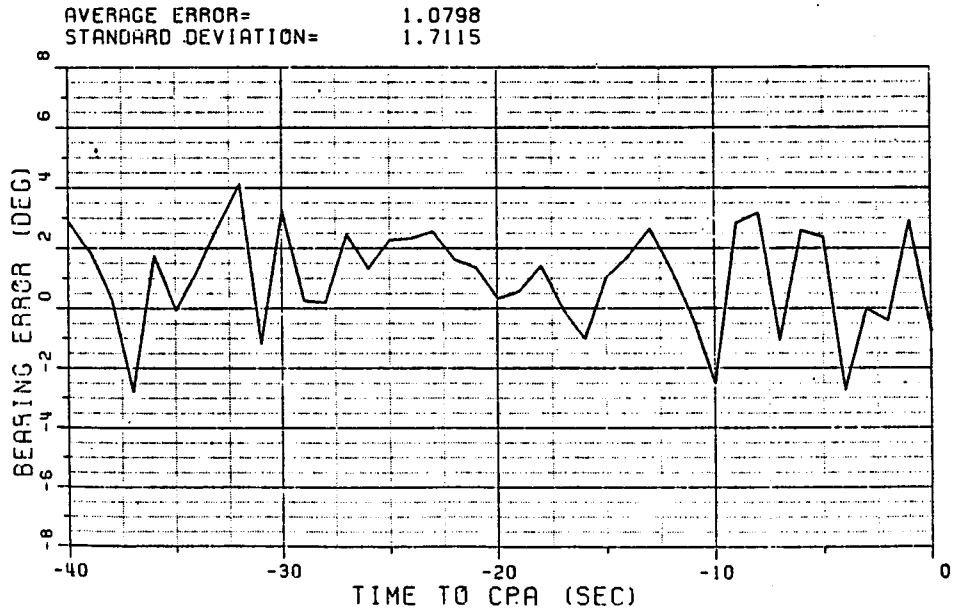

Figure 31. Bearing errors on Path One with noise and scattering effects.

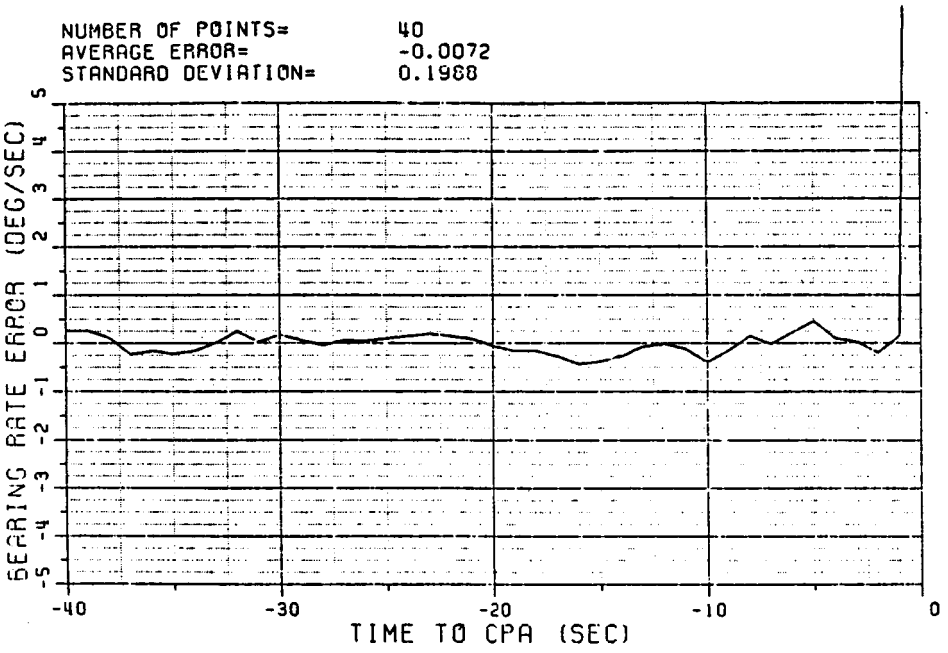

Figure 32. Bearing rate errors on Path One with noise and scattering effects.

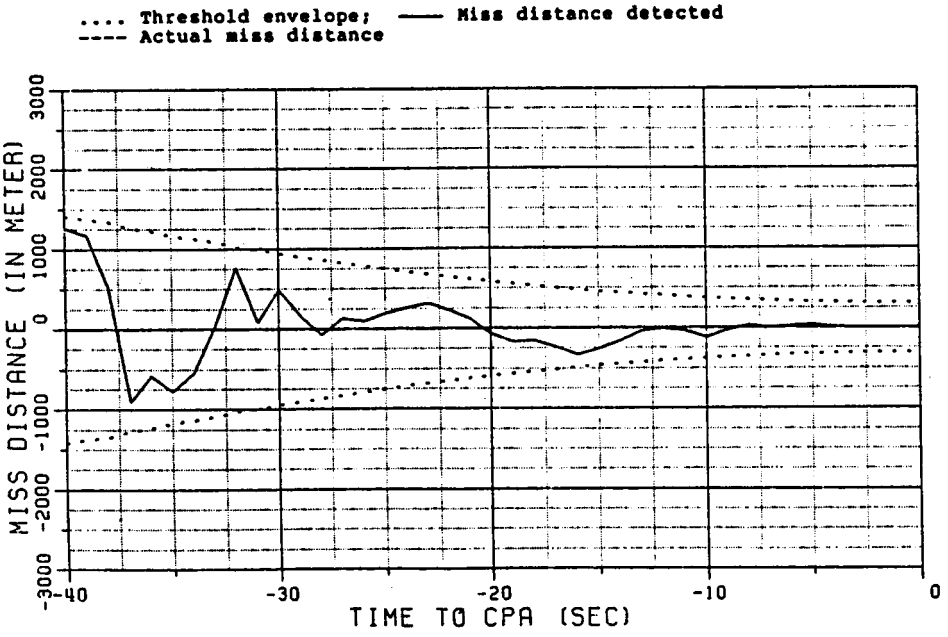

Figure 33. Threshold and miss distance curves on Path One with noise and scattering effects.

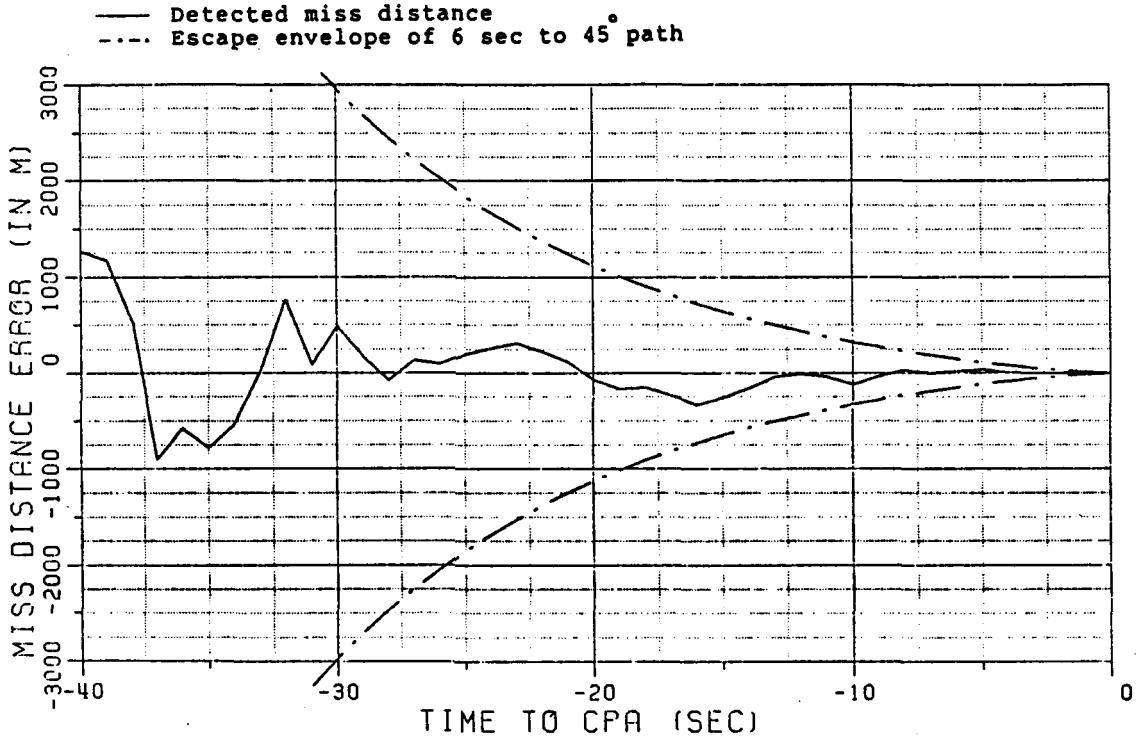

Figure 34. Miss distance error curve on Path One with noise and scattering effects.

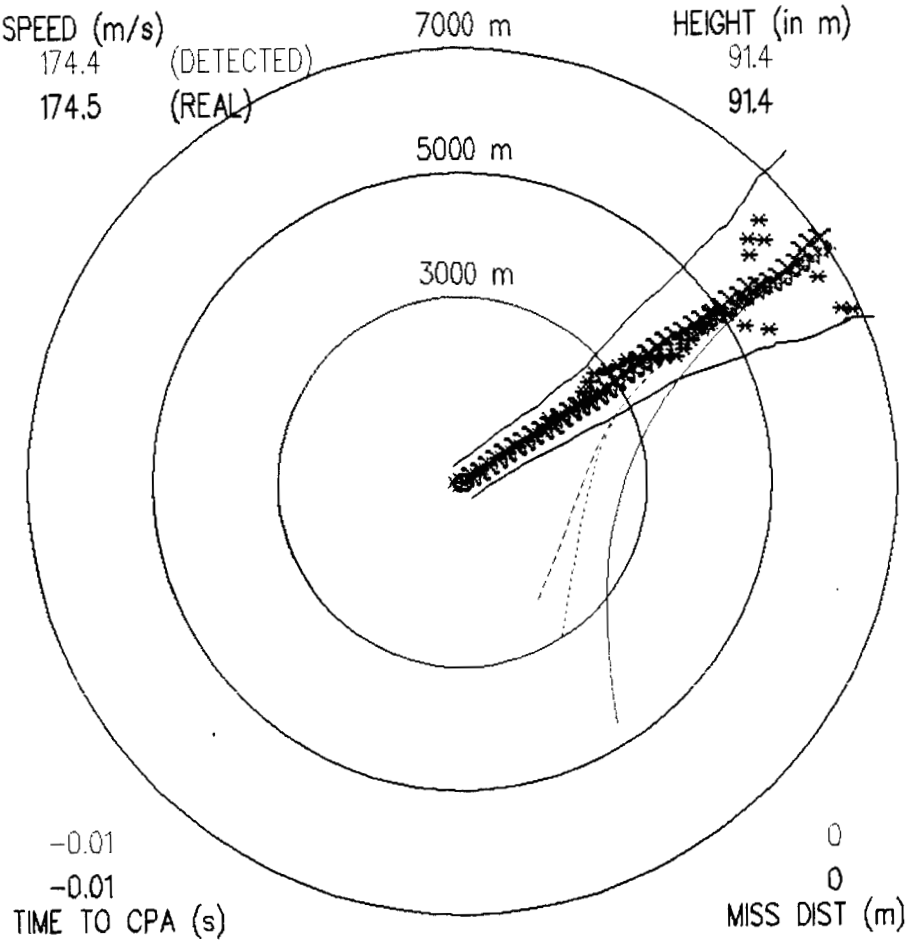

Figure 35. The graphic display of Path One with noise and scattering effects.

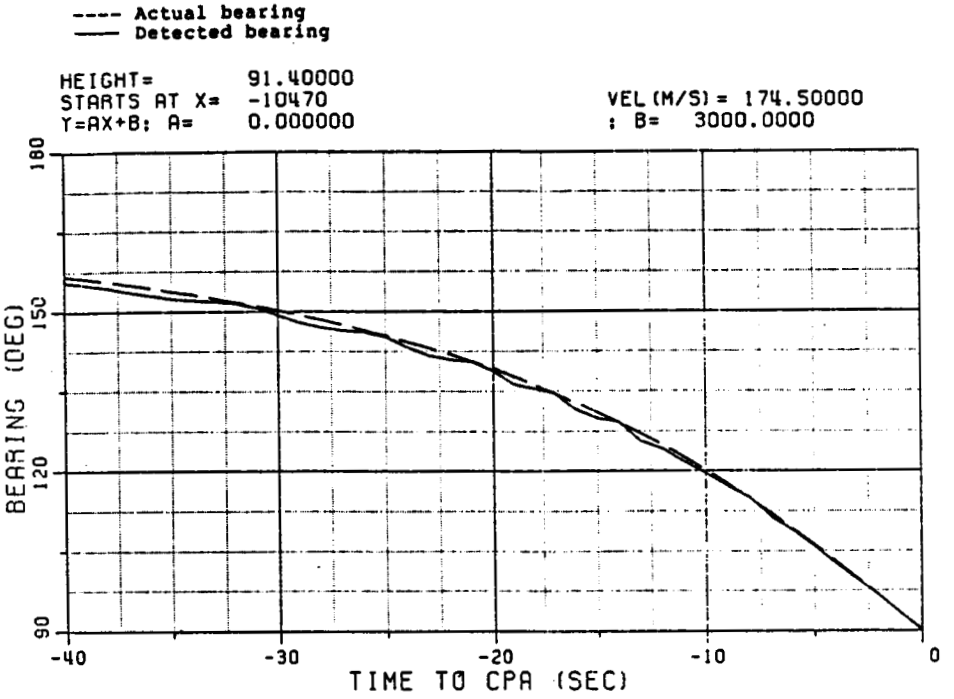

Figure 36. Actual and detected target bearing on Path Two with only scattering effects.

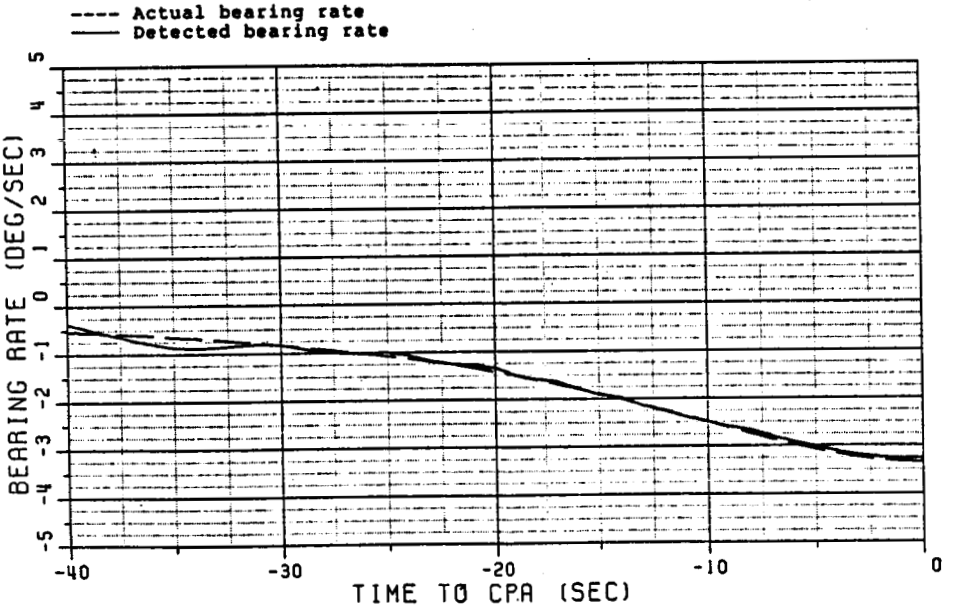

Figure 37. Bearing rate curve on Path Two with only scattering effects.

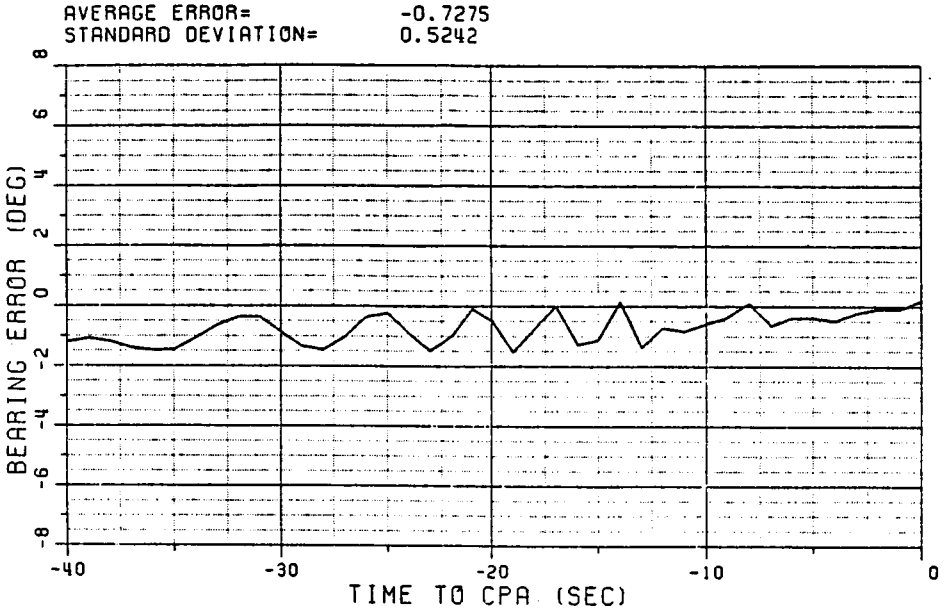

Figure 38. Bearing error curve on Path Two with only scattering effects.

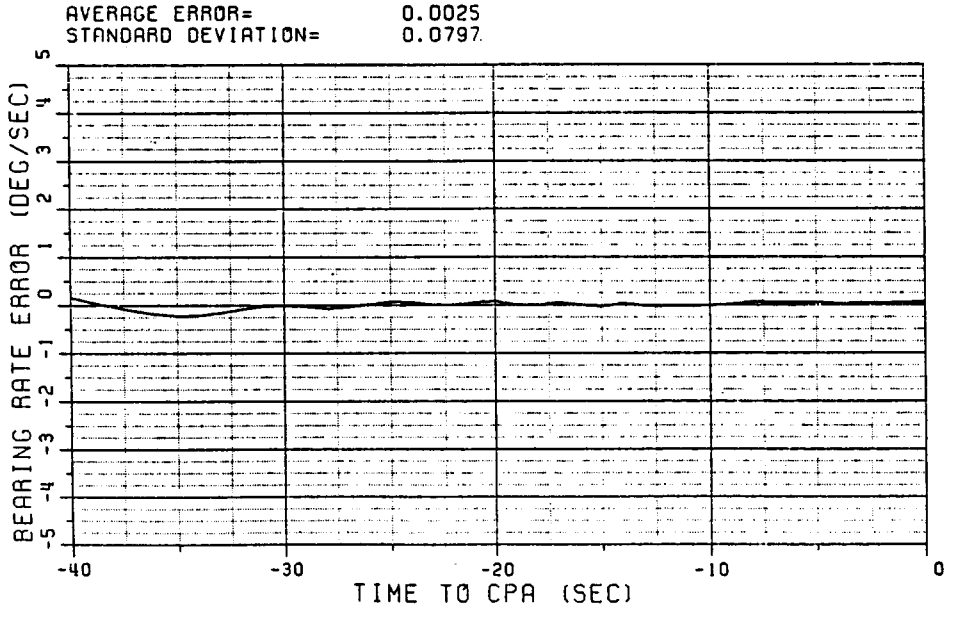

Figure 39. Bearing rate error curve on Path Two with only scattering effects.

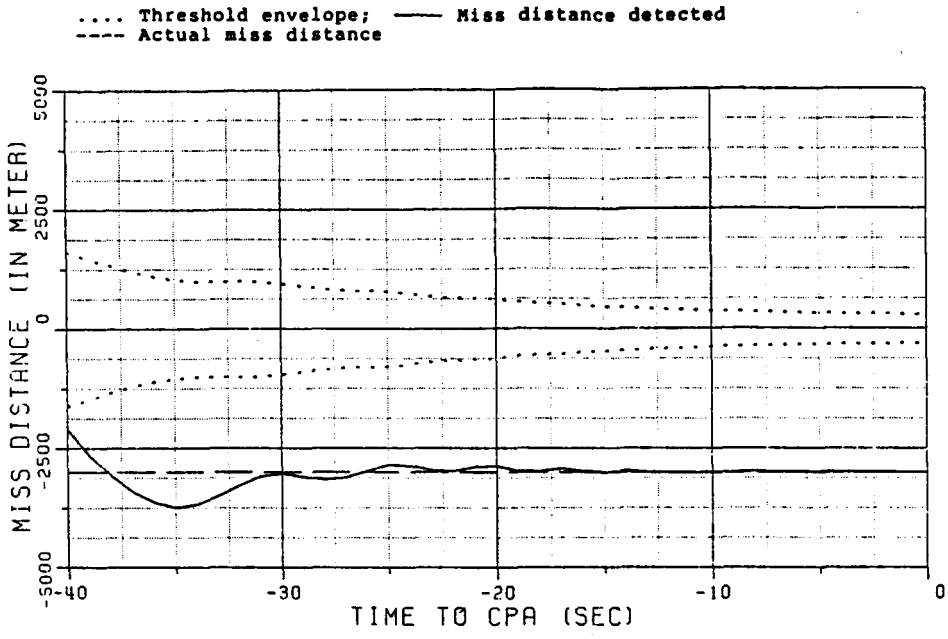

Figure 40. Threshold and miss distance curves on Path Two with only scattering effects.

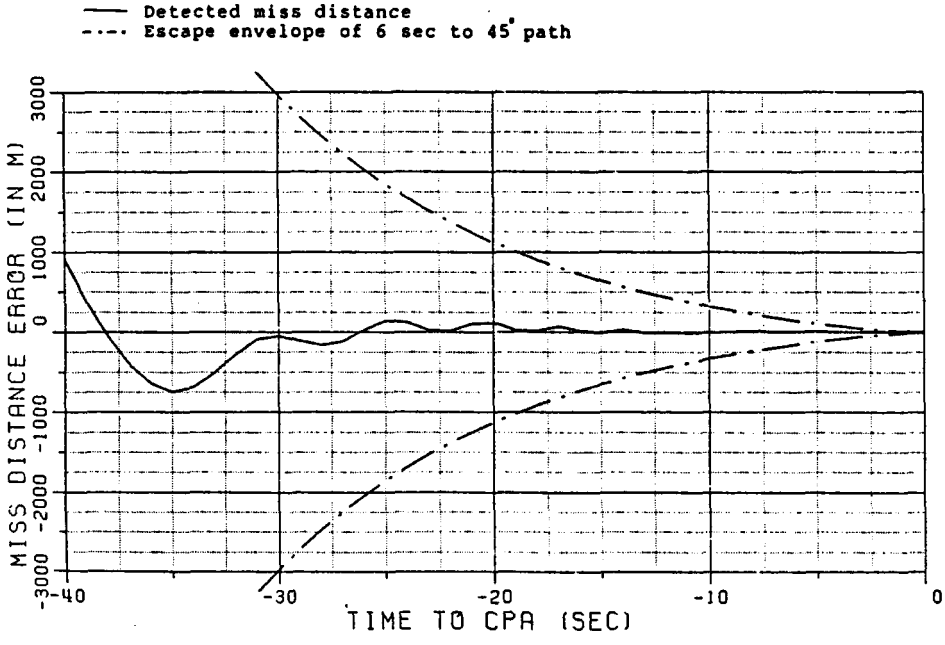

Figure 41. Miss distance error curve on Path Two with only scattering effects.

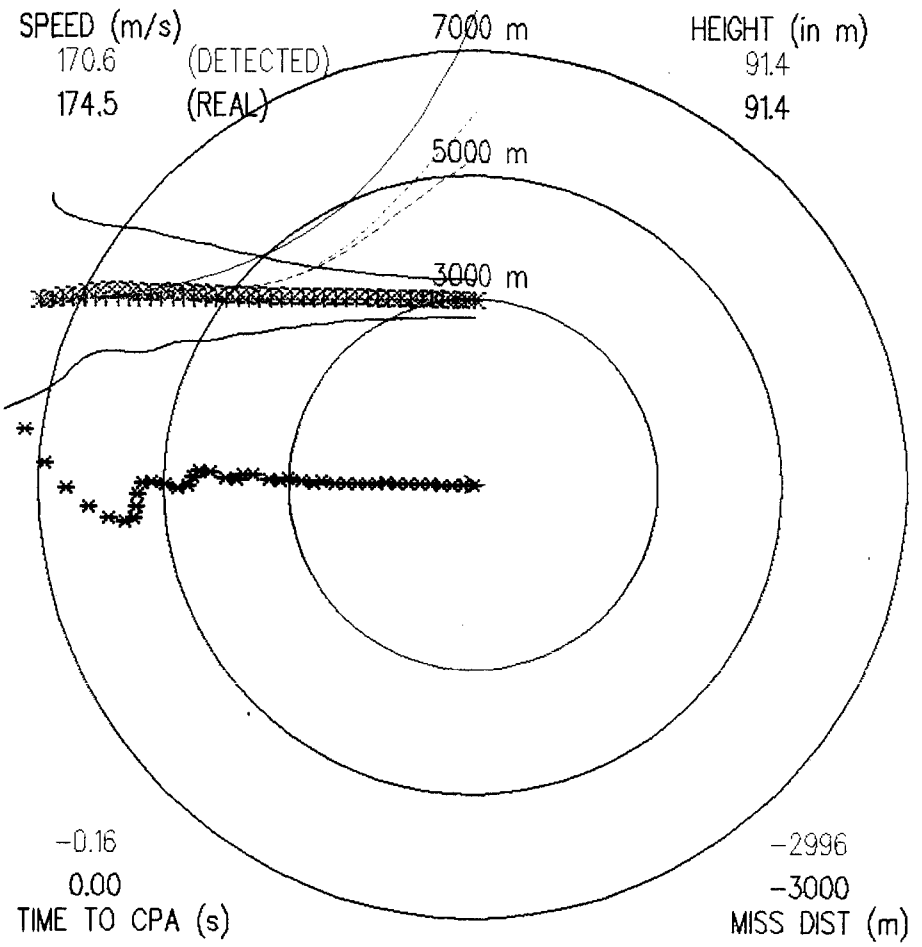

Figure 42. The graphic display of Path Two with only scattering effects.

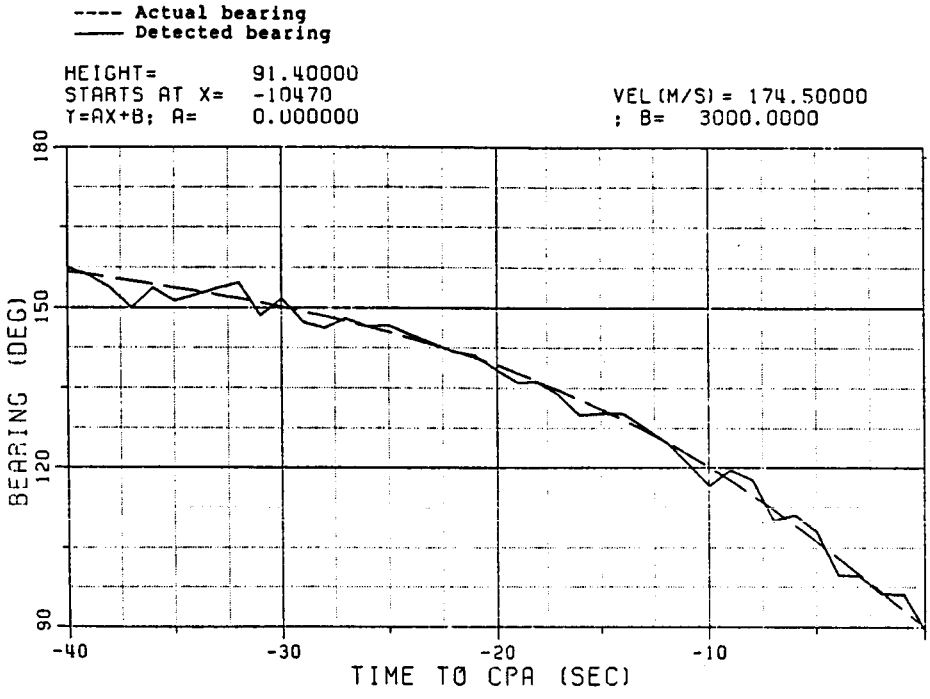

Figure 43. Target bearing curve on Path Two with noise and scattering effects.

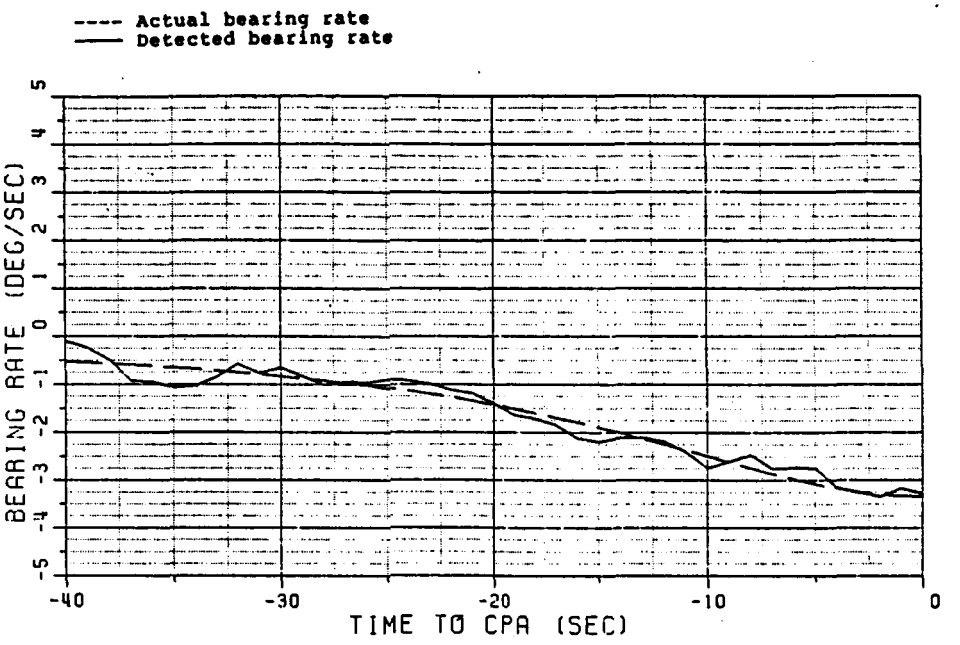

Figure 44. Bearing rate curve on Path Two with noise and scattering effects.

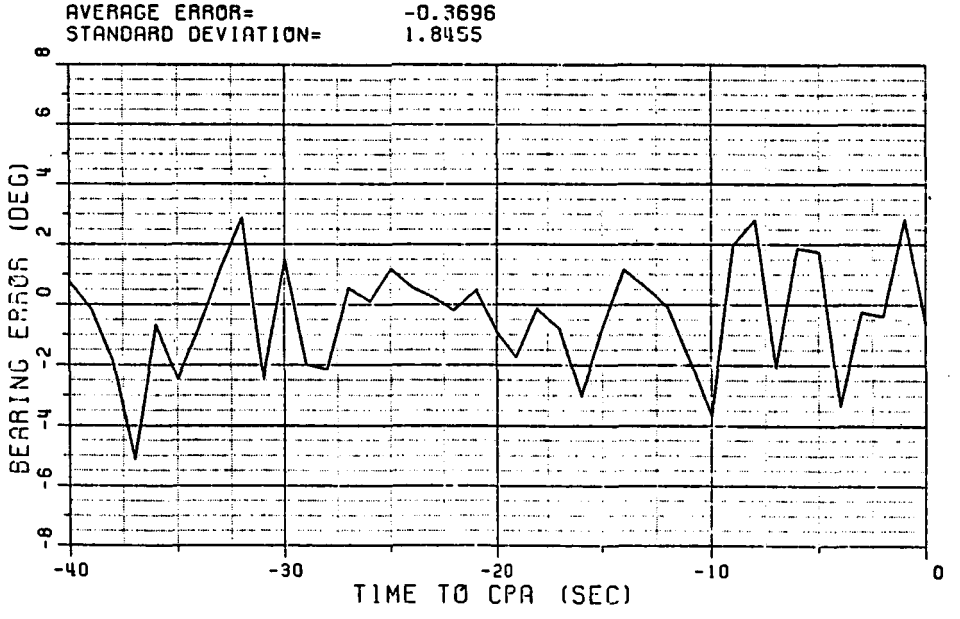

Figure 45. Bearing error curve on Path Two with noise and scattering effects.

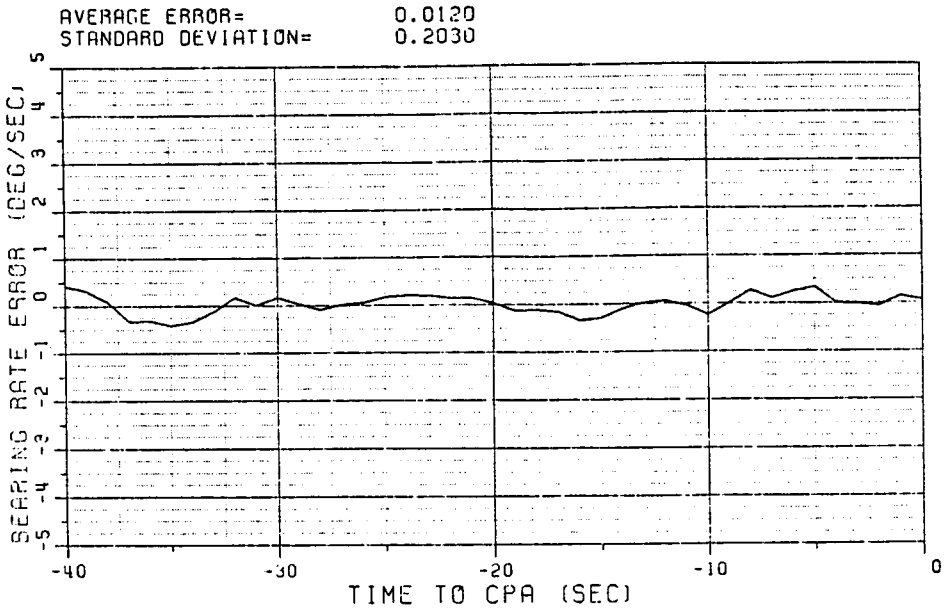

Figure 46. Bearing rate error curve on Path Two with noise and scattering effects.

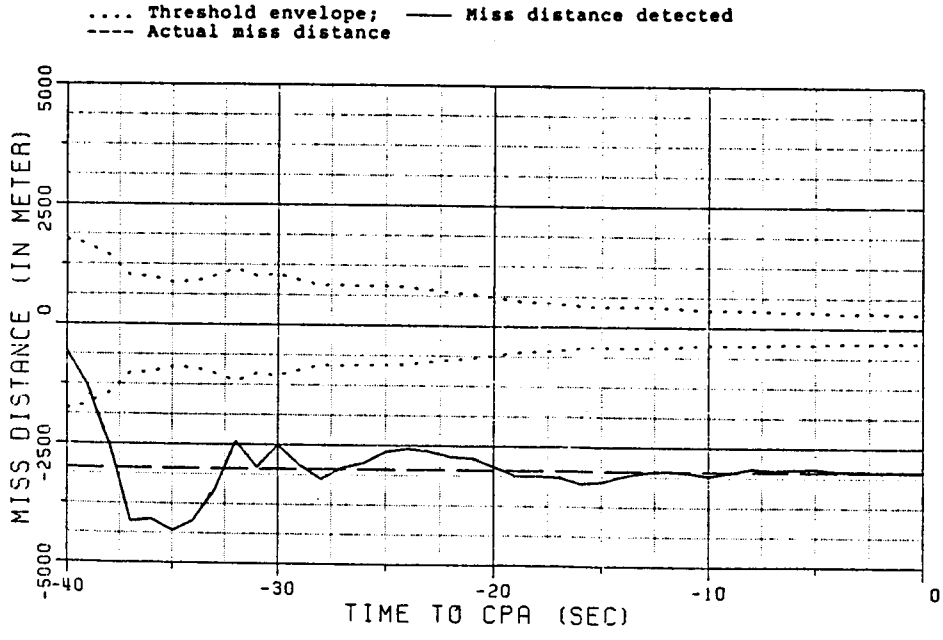

Figure 47. Threshold and miss distance curves on Path Two with noise and scattering effects.

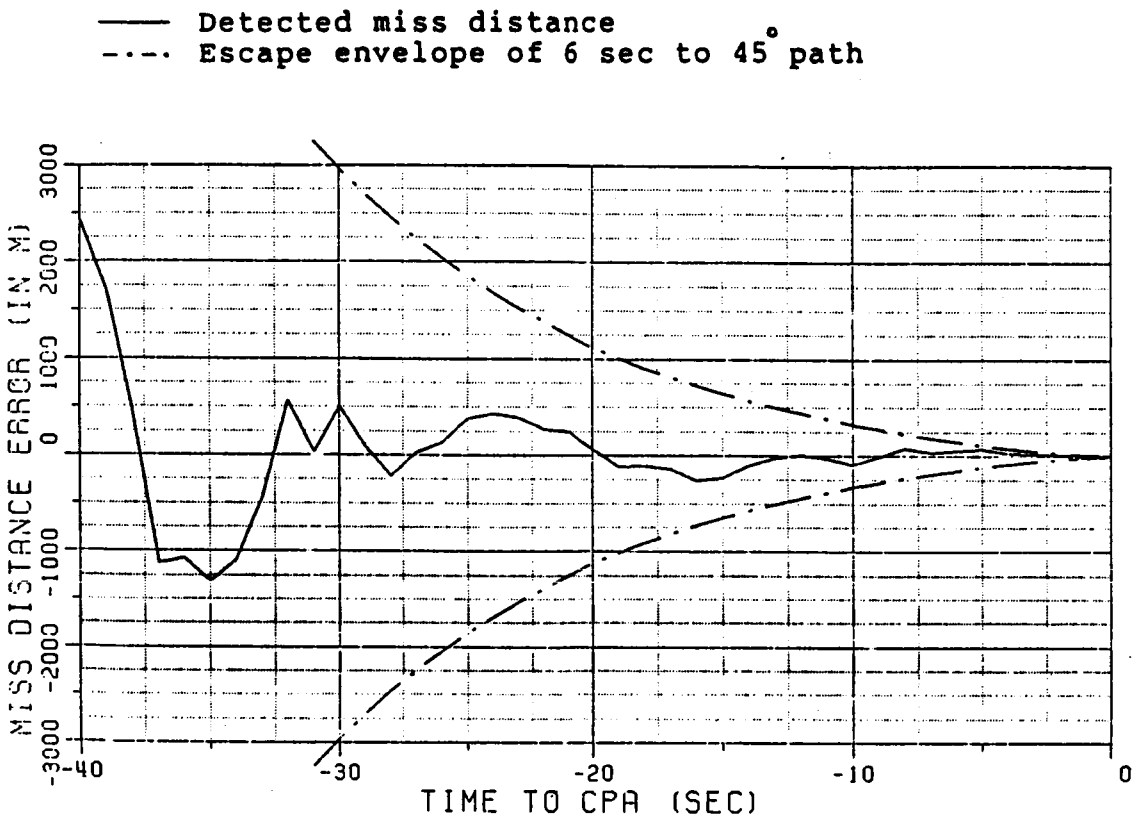

Figure 48. Miss distance error curve on Path Two with noise and scattering effects.

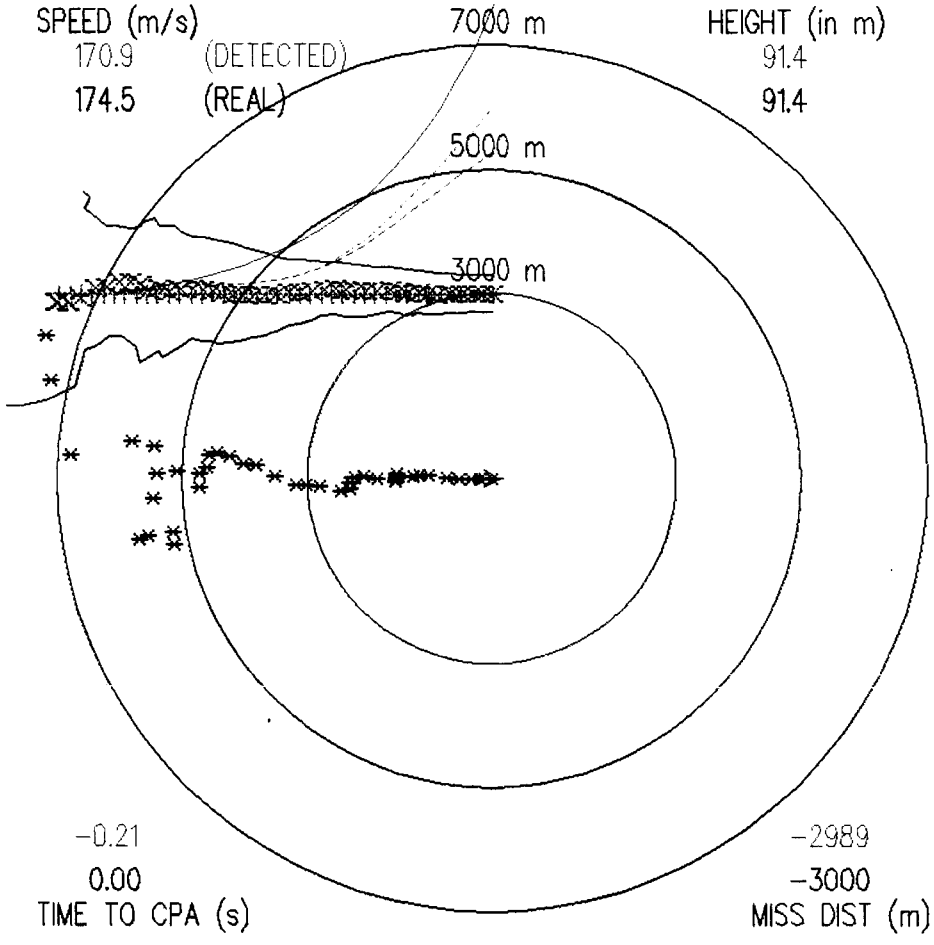

Figure 49. The graphic display of Path Two with noise and scattering effects.

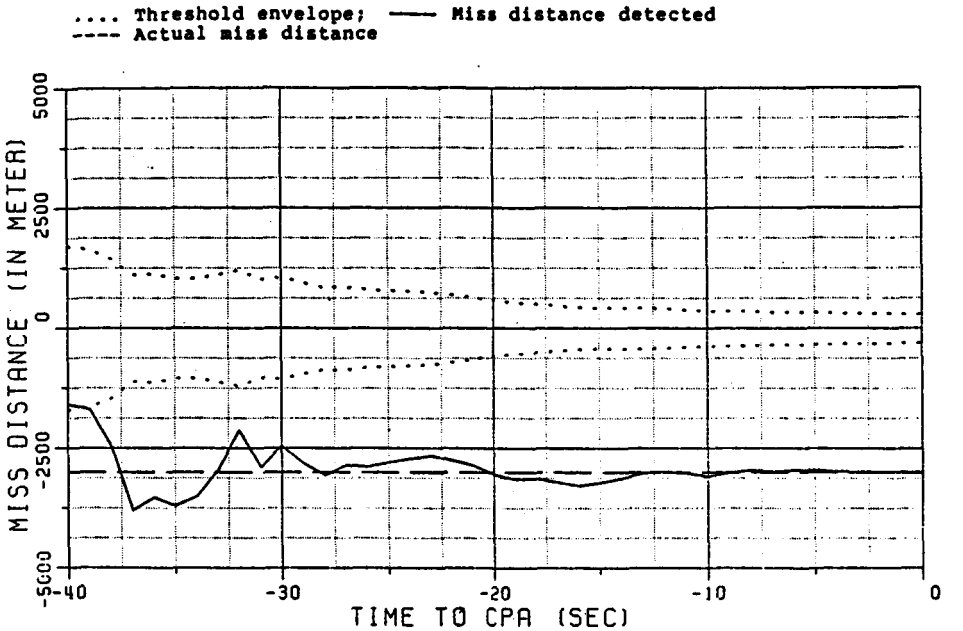

Figure 50. Threshold and miss distance curves on Path Two with noise alone.

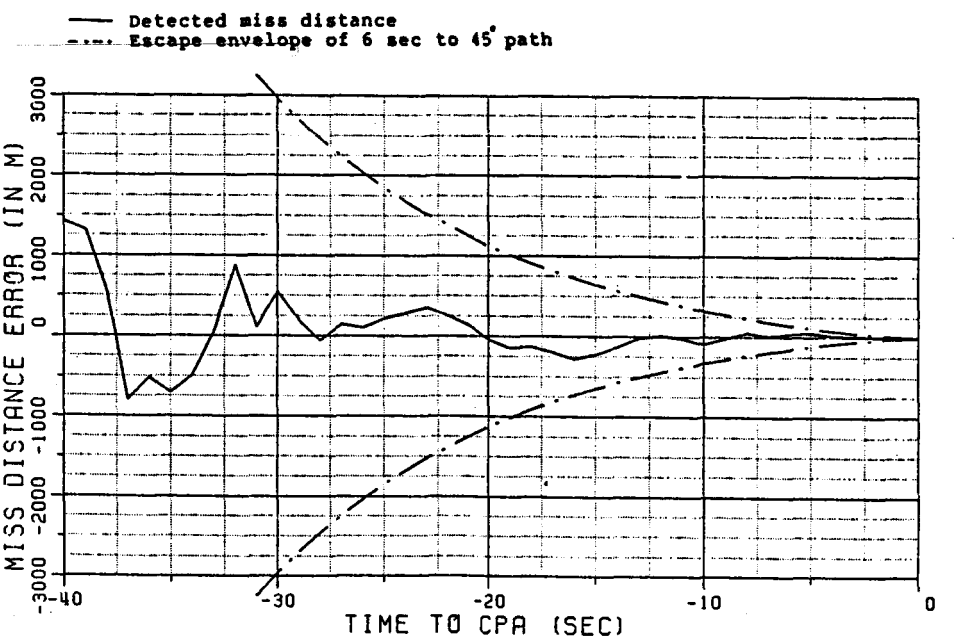

Figure 51. Miss distance error curve on Path Two with noise alone.

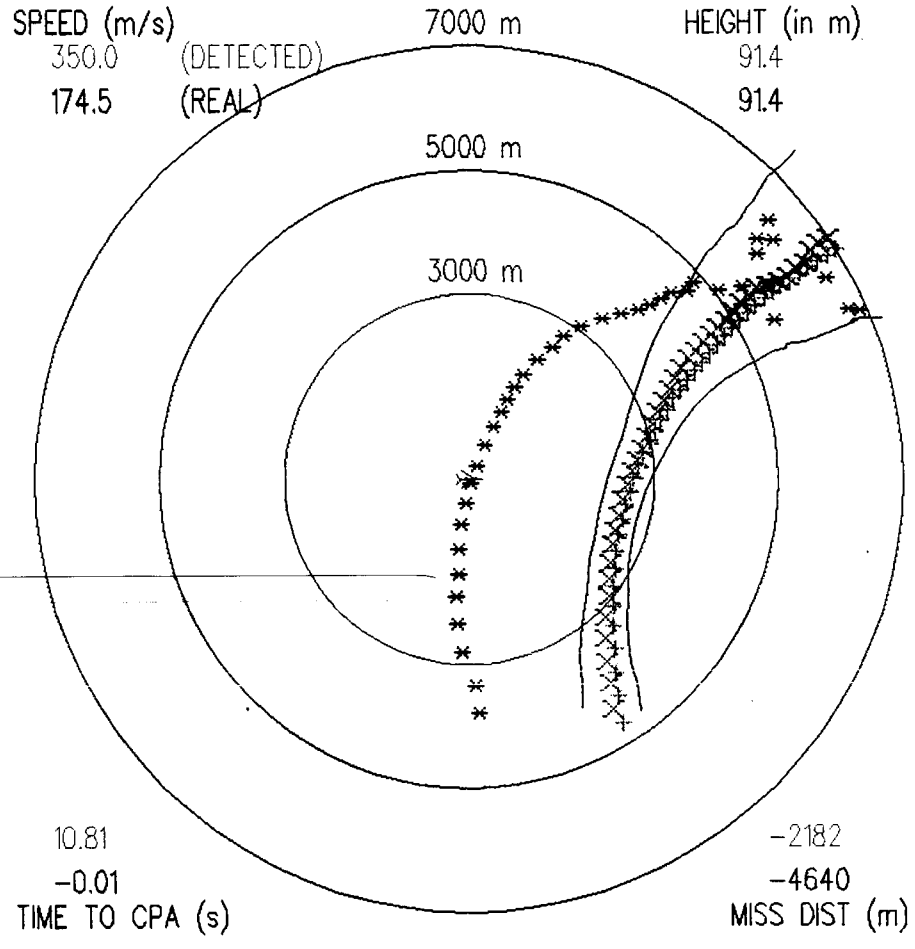

Figure 52. The graphic display after the protected aircraft has taken an escape curves on Path One.

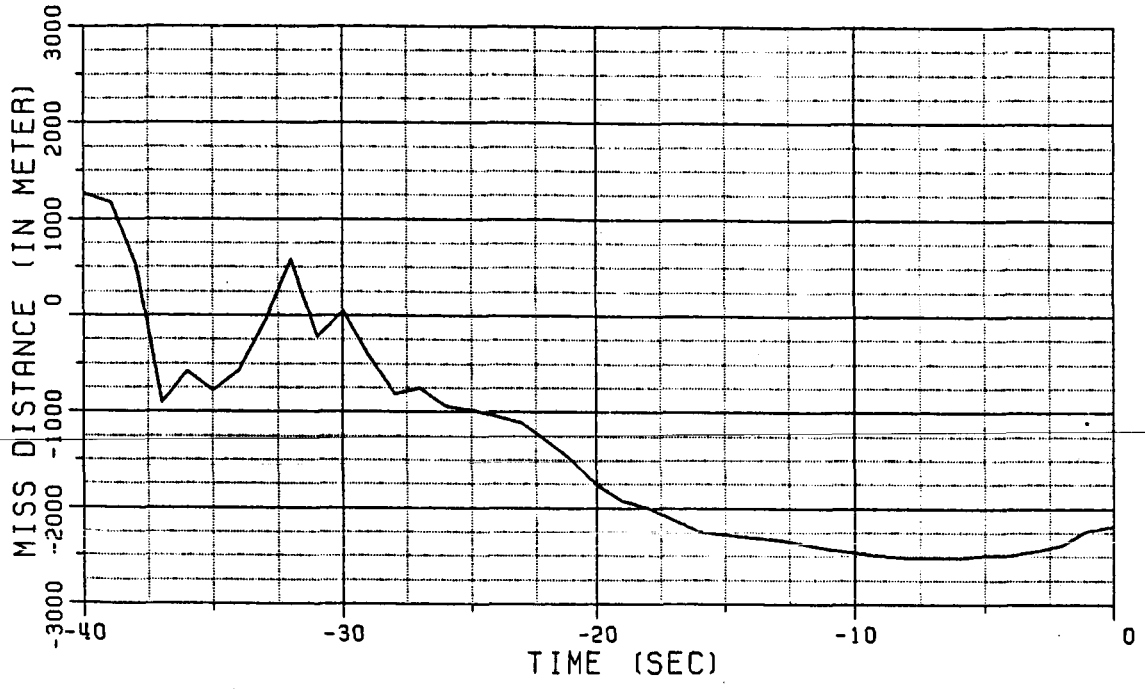

Figure 53. Detected miss distance (corresponding to Figure 52) after the protected aircraft has taken an escape curve.

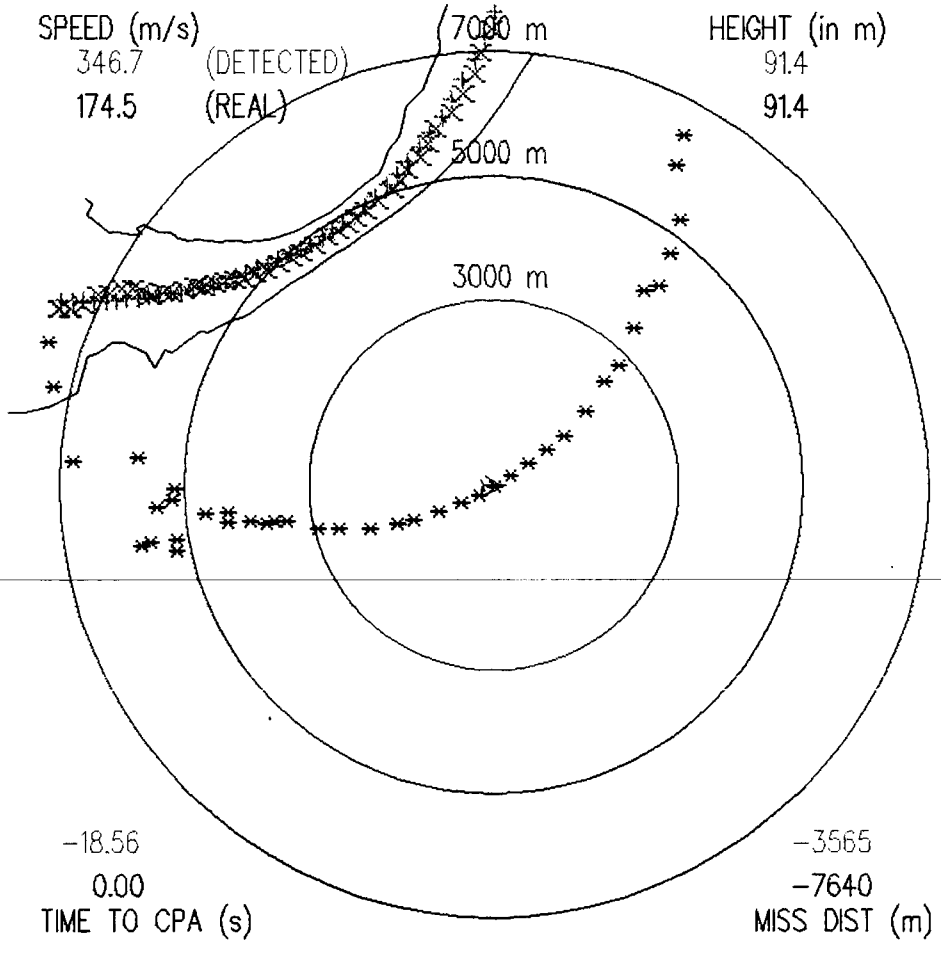

Figure 54. The graphic display after the protected aircraft has taken an escape curve on Path Two.

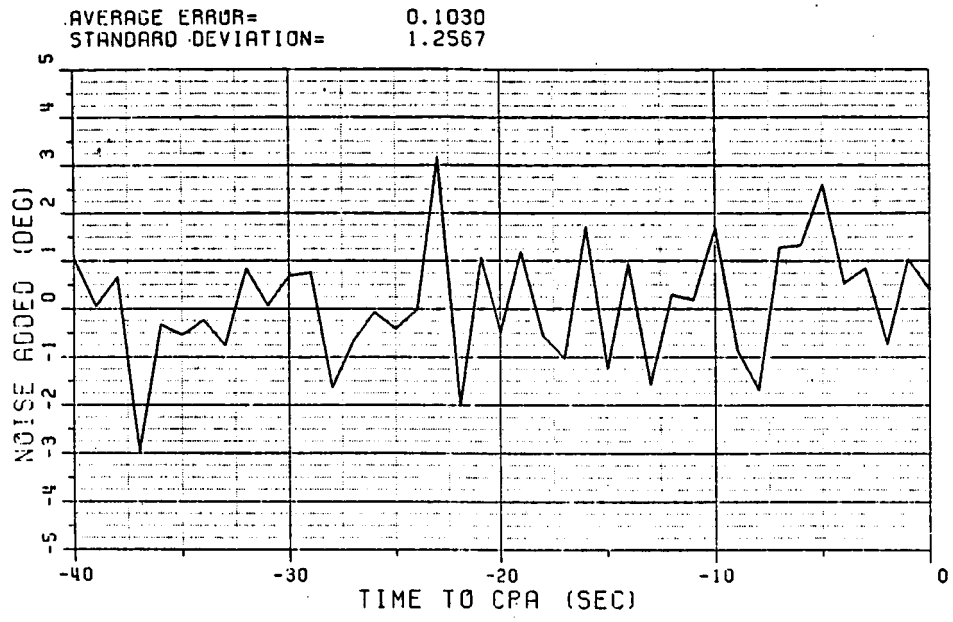

Figure 55. Second noise curve added on Path One.

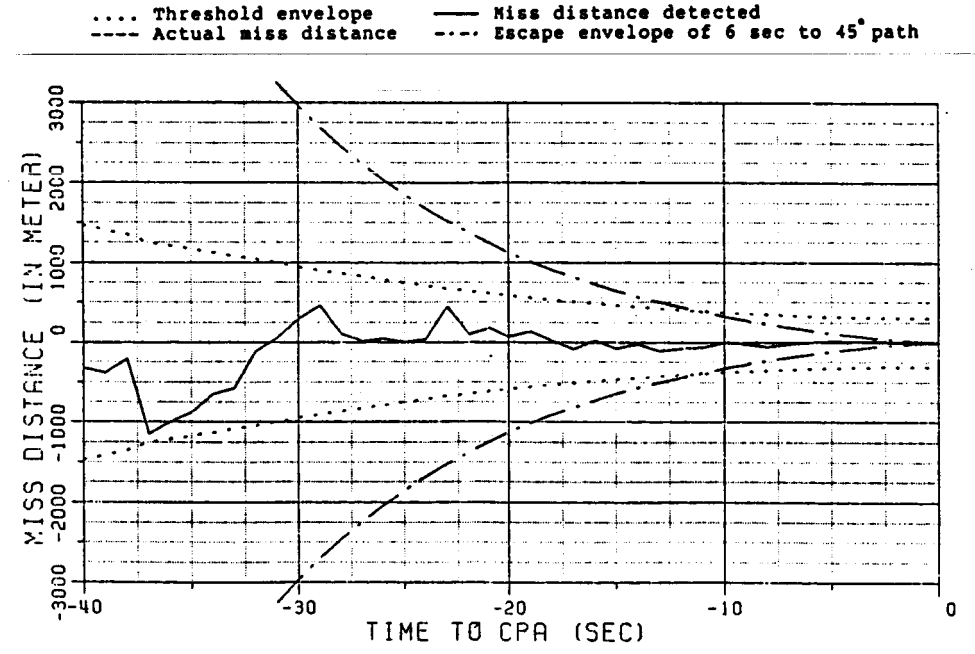

Figure 56. Resulting miss distance error curve on Path One.

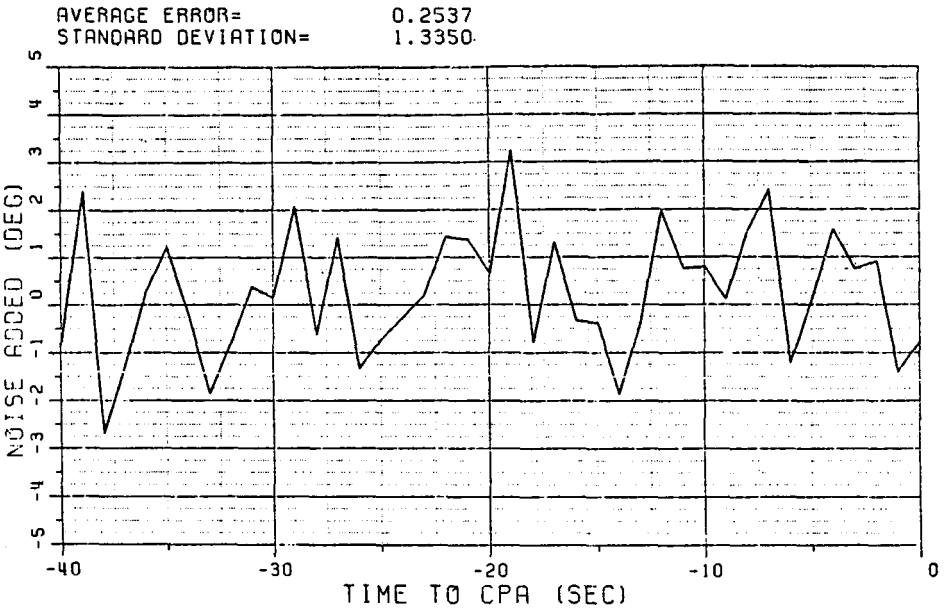

Figure 57. Third noise curve added on Path One.

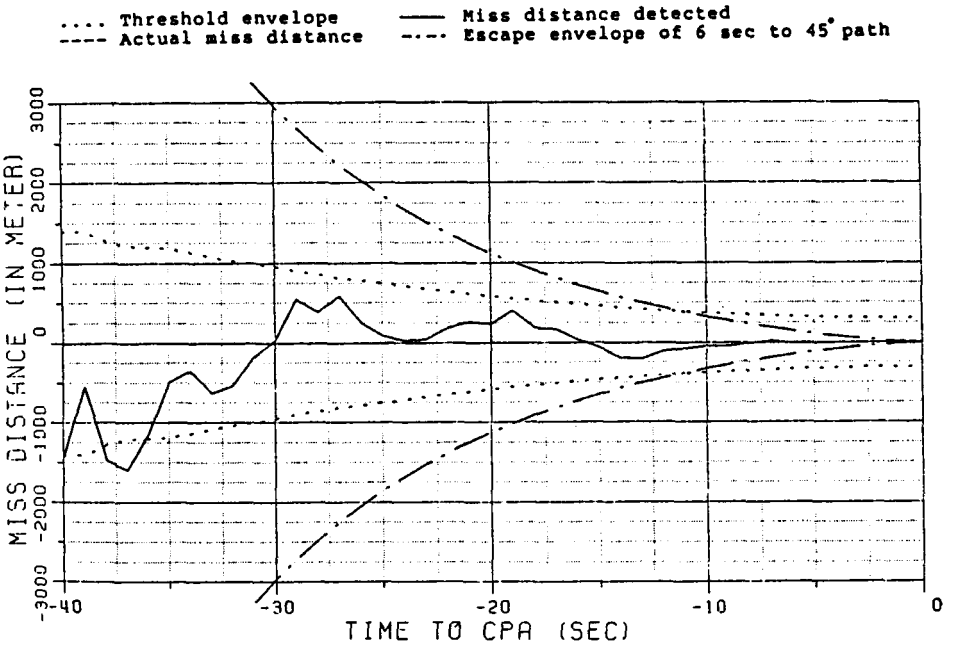

Figure 58. Resulting miss distance error curve on Path One.

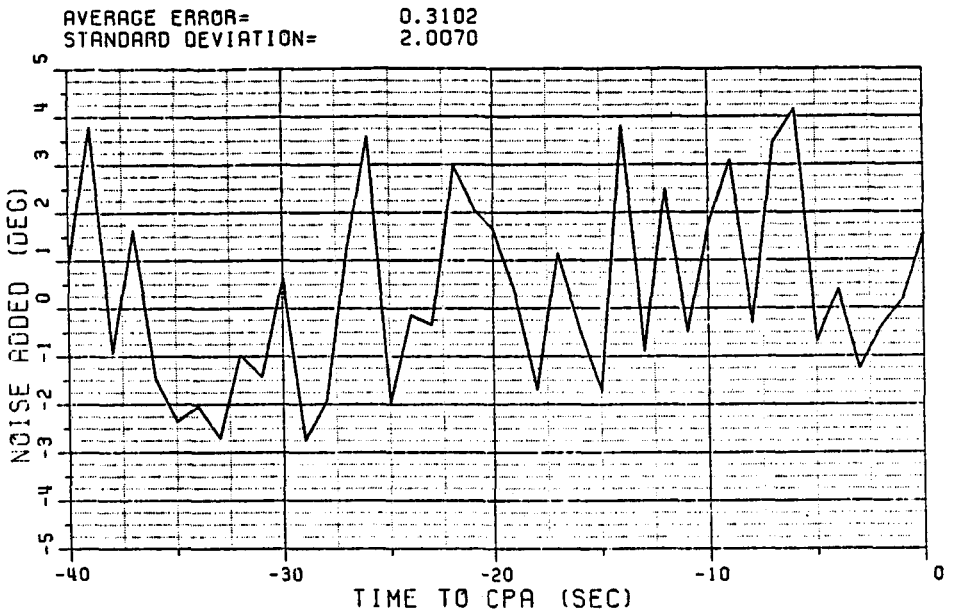

Figure 59. Fourth noise curve added on Path One.

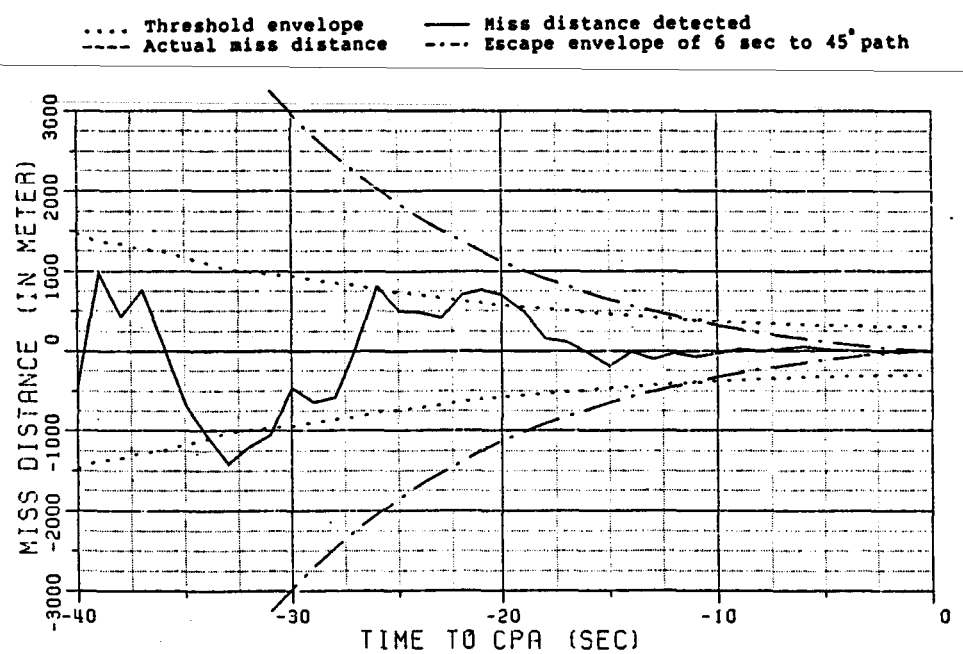

Figure 60. Resulting miss distance error curve on Path One.

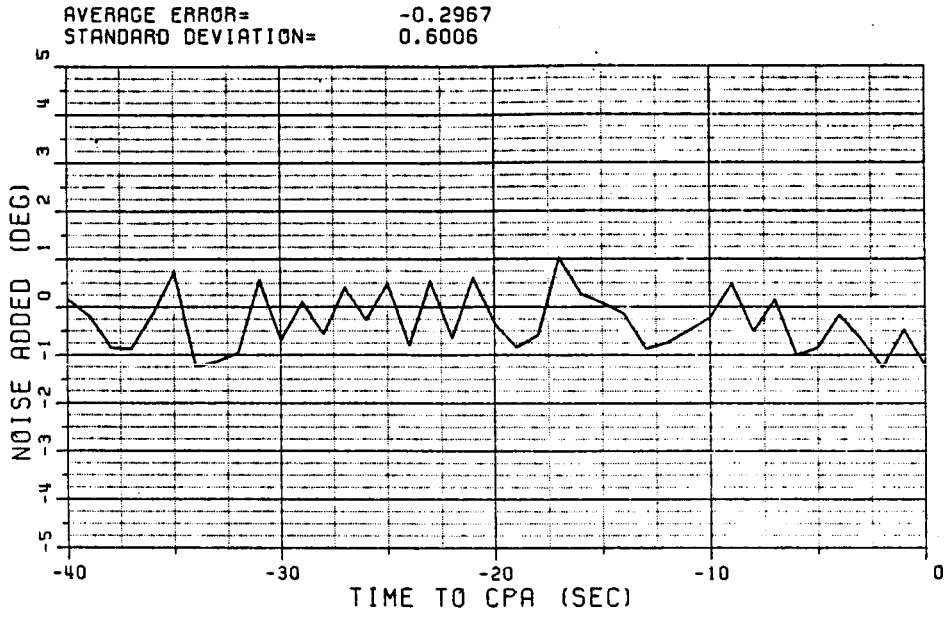

Figure 61. Fifth noise curve added on Path One.

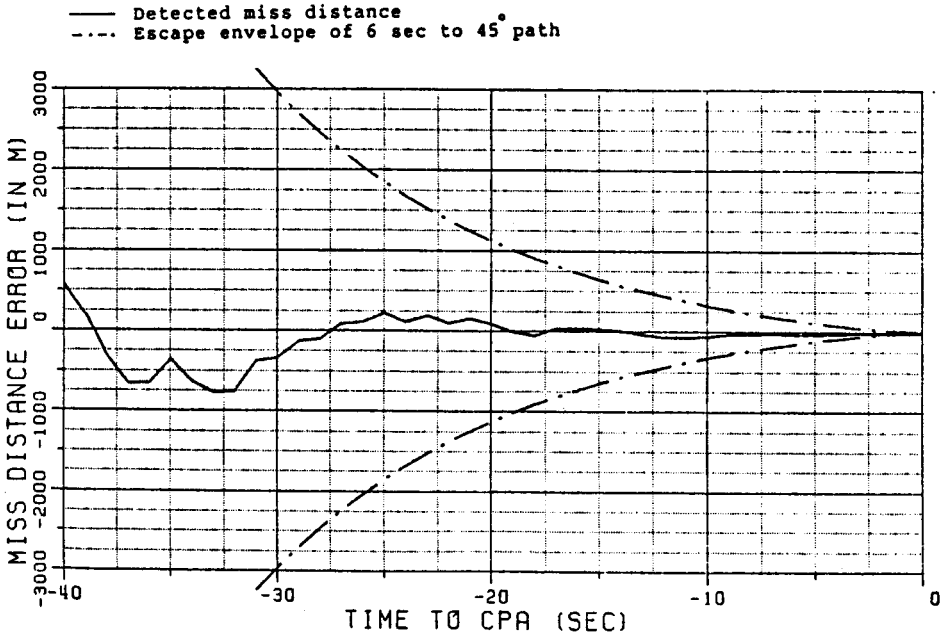

Figure 62. Resulting miss distance error curve.

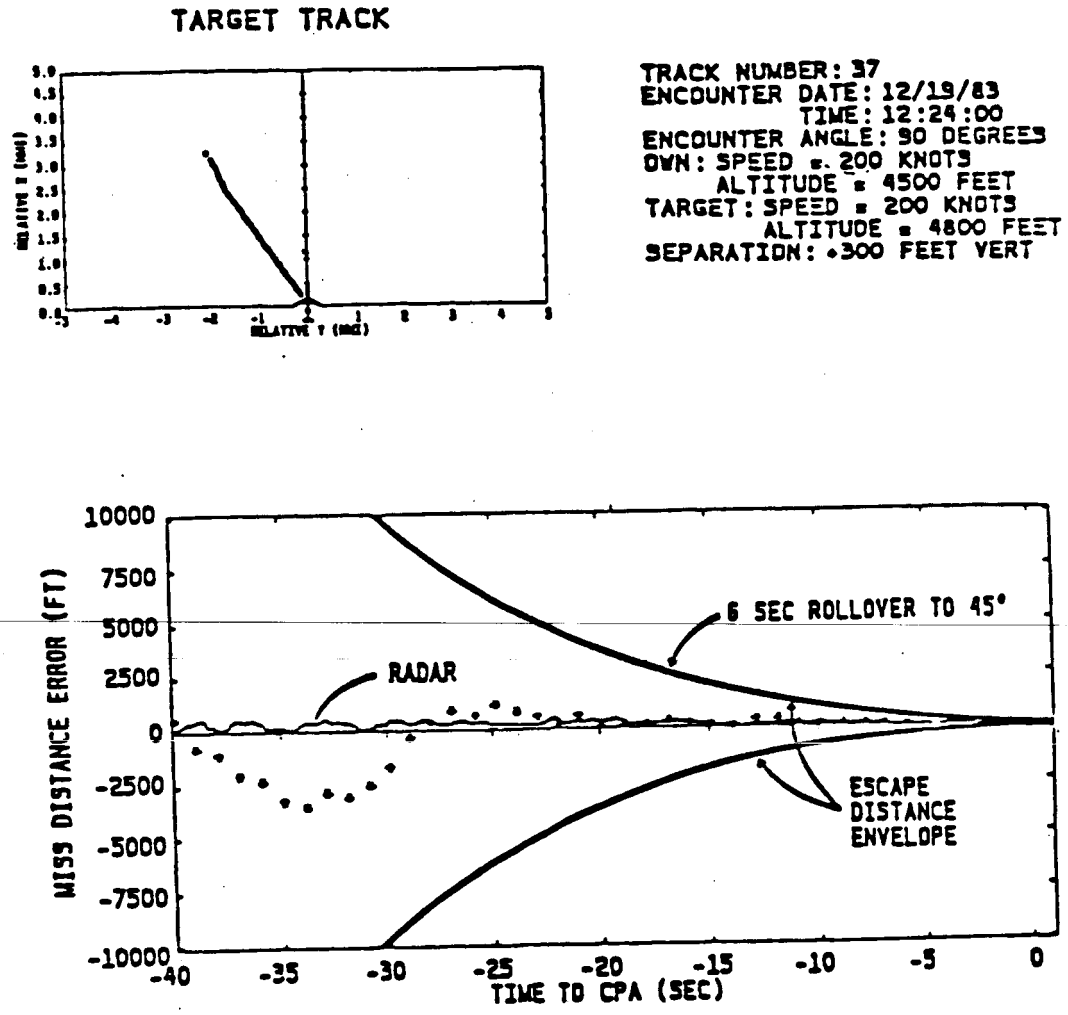

Figure 63. Results of a flight test conducted by Bendix Corporation, obtained from Reference [9].

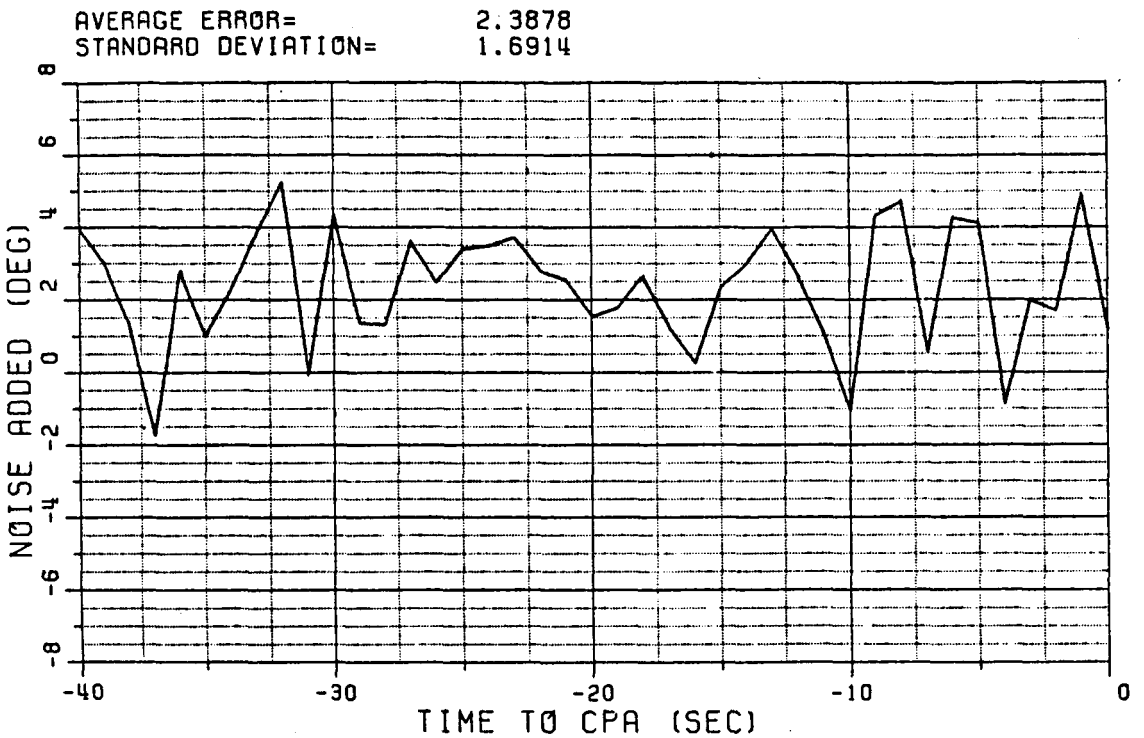

Figure 64. Noise added to Path One. Note that this noise curve has been increased by 2° as compared to Figure 28.

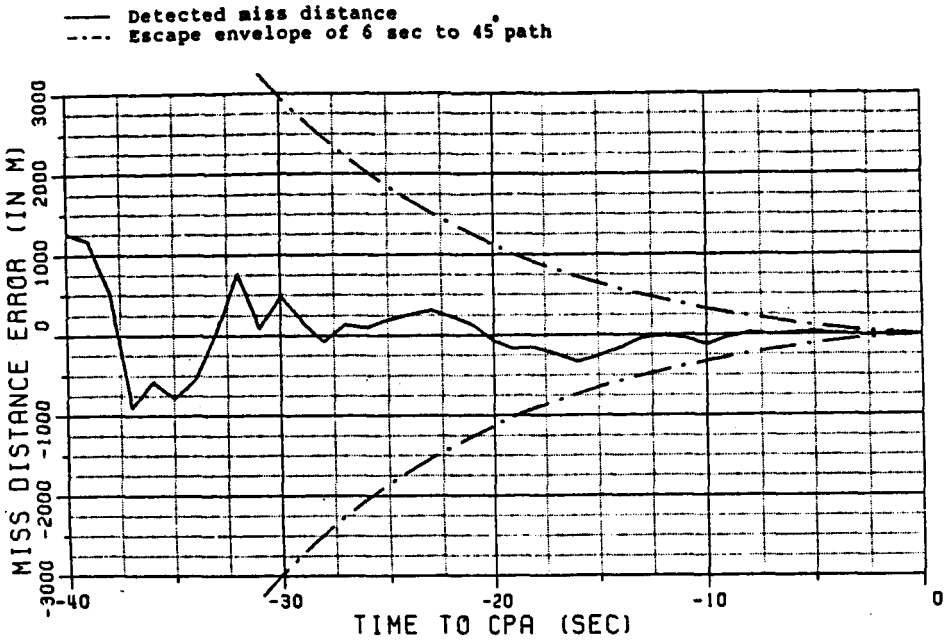

Figure 65. Resulting miss distance error curve on Path One.

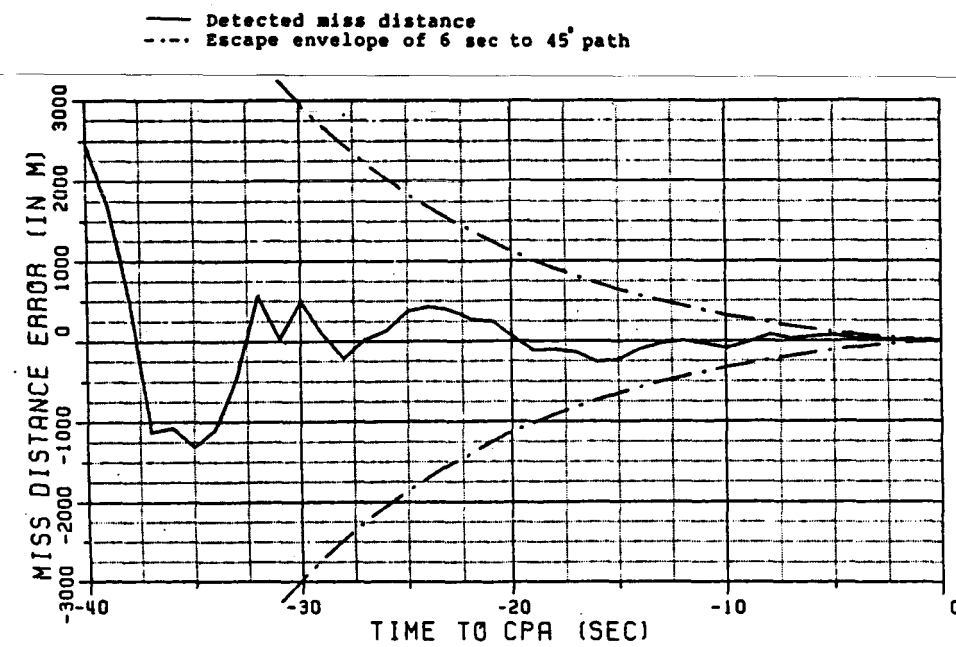

Figure 66. Resulting miss distance error curve on Path Two.